UCLA ENG-8746
December 1987

UTILIZATION OF FEP ENERGETICS

FINAL REPORT

December 31, 1987

by

T. H. K. Frederking, Principal Investigator
P. Abbassi
F. Afifi
P.K. Khandhar
D. Y. Ono
W. E. W. Chen

PREPARED FOR THE
NATIONAL AERONAUTICS AND SPACE ADMINISTRATION
AMES RESEARCH CENTER
MOFFETT FIELD, CA 94035

Grant NAG 2-464

Department of Chemical Engineering
School of Engineering and Applied Science
University of California, Los Angeles, CA 90024

UCLA ENG-8746
December 1987

UTILIZATION OF FEP ENERGETICS

FINAL REPORT

December 31, 1987

by

T. H. K. Frederking, Principal Investigator
P. Abbassi
F. Afifi
P.K. Khandhar
D. Y. Ono
W. E. W. Chen

WITH APPENDIX SECTIONS BY S. Caspi, S.W.K. Yuan et al.

PREPARED FOR THE
NATIONAL AERONAUTICS AND SPACE ADMINISTRATION
AMES RESEARCH CENTER
MOFFETT FIELD, CA 94035

Grant NAG 2-464

Department of Chemical Engineering
School of Engineering and Applied Science
University of California, Los Angeles, CA 90024

TABLE OF CONTENTS

1. ABSTRACT

The R&D work on Fountain Effect Pump systems (FEP systems) has been of interest in the competition between mechanical pumps for He II and FEP units. The latter do not have moving parts. In the course of the work, the energetics has been addressed using one part of a simple "4-changes of state" cycle. One option is the FEP ideal change of state at constant chemical potential (μ). The other option is the two-state sequence μ–P with a $d\mu = 0$ state change followed by an isobar. Questions of pump behavior, of flow rate response to temperature difference at the "hot" end, and related questions of thermodynamic cycle completion and heat transfer have been addressed. Porous media data obtained elucidate differences between vapor-liquid phase separation (VLPS) and Zero Net Mass Transfer (ZNMF).

2. INTRODUCTION

The project has been started up with the goal of quantification of the energetics of fountain effect pump systems (FEP systems) which utilize the thermomechanical effect in liquid He II in the superfluid range. Mostly 1.2 to 2.1 K is a rough characterization of temperatures of interest in various large scale systems. In the course of the work it became clear that the topics ought to include both the equilibrium state thermodynamics and the transport phenomena of the process components. The emphasis has been on micro-gravity noting that the first explicit successful use of thermomechanical forces (TM forces) has been in space vessels in vapor liquid phase separators (VLPS). The IRAS system has become famous in this respect. The ongoing efforts focusing on additional controlled fluid management reach out farther. An example is the transfer of liquid in space using the FEP type systems without moving parts. Prior to a detailed inspection it appears to be useful to focus on historical developments.

1988 may be considered the half century jubilee year for superfluidity research and development. Though indications, such as the lambda transition in liquid Helium-4, have been known since Dana and Onnes work, the systematic study of superfluidity did not start before about 1938. In that year the thermomechanical effect had been reported by Allen and Jones[1]. Nearly simultaneously, superfluidity was found, i.e. the ability of He II to flow through very narrow channels. These findings had been the subject of sort of a race as both Kapitza[2] and Allen and Misener[3] got data in the area of inquiry. Concomitantly the two-fluid model came along with a surprising speed in view of entirely new phenomena, the "supereffects" of He II. In particular, the London version became accessible to Western researchers while the Landau version remained in the Eastern domain at first. Thus, major theoretical developments gave immediate support to data interpretation efforts.

It did not take long time, after the advent of the Collins liquefier, to launch demonstrations of the fountain effect, and of the static version of the thermomechanical effect, in major universities having "Collins" systems. Thus, many additional phenomena of the underlying physics got significant attention. An example is the resolution of first sound in He II, the usual pressure density disturbance propagation, and of second sound, the temperature entropy mode. Other sounds modes followed e.g. third sound, fourth sound and fifth sound.

A comprehensive program of research had been started by Hammel and Keller[4] in the area of He II film flow and in thermodynamics and transport phenomena. In particular very fine slits were used to see the fountain effect thermostatics. According to London's equation, the thermomechanical pressure increment is given by

$$dP = \rho\ S\ \ dT \tag{2.1}$$

S = entropy per unit mass, ρ density.

Therefore, the difference in pressure due to a temperature difference Δ T is

$$\Delta P = \int \rho\ S\ \ dT \tag{2.2}$$

In the context of this equation, Hammel and Keller obtained limits imposed on the maximum value of ΔP attainable. Also critical velocities appeared to be an obstacle toward immediate full utilization of the pressure difference predicted by equation (2). Indeed kinetic energy effects had to be taken into account. An example used in the two-fluid frame of equations is

$$\nabla(\mu + v_s^2/2) = 0 \tag{2.3}$$

The kinetic energy, per unit mass, of flowing superfluid is $v_s^2/2$; μ is the chemical potential per unit mass, v_s superfluid velocity. The entire set of data has not been easily accessible to simple theory as there were numerous critical velocity values for various modes. In this context,

the entropy was checked in detail because of concerns of entropy contributions not assigned to normal fluid alone. Nevertheless, a special mode called zero net mass flow was among the early systems studied. It turned out that He II had an enormous axial heat transport capability despite operation in the "supercritical" regime, i.e. beyond the critical velocity. Thus, the thermomechanical forces (TM forces) appeared to be at work, and interesting arrangements were created to take advantage of this type of "heat piping" properties of He II. Thus, in a sense, the "first use" of VLPS, as an application of He II TM forces, has been superseded in a subtle manner by the laboratory use of zero net mass flow conditions.

Coming back to devices, it is noted that F. London[5] already looked at thermodynamic state changes of a special system. One may consider this a "thought experiment". One may also look at this as a first proposal for a system with the potential of practical realizability. In 1938 things were very far away from such a status. In fact occasionally the opinion had been voiced that Equation (2) does not provide a significant incentive for practical use. The argument goes as follows: The critical velocities are mostly very low; the pressure difference attainable at the critical velocity is not large; further, the energy input in the form of heat does not provide for a "very efficient" system from the second law of thermodynamics point of view. These arguments contain some truth however they ignore several extremely interesting features for the space fluid management.

First of all, the low ΔP and low critical velocity may be overcome by suitable very fine porous plugs and in particular by multi-stage pump systems. Such a system did not come up before the Eighties. Severijns[6] demonstrated the use of a 4-stage pump which had very good agreement with predictions based on Equations (1) and (2). The second major point is the option of using "waste heat" as input, for instance parasitic heat inputs available through most cryogenic insulation systems e.g. in supports, current leads and others. The second law of thermodynamics is valid. However it provides more of a comparative measure for various

schemes, considered competitors, than a serious limitation on the "waste heat" use. Last not least, the question of realiability, by elimination of as many moving parts as possible, is another factor. The FEP unit permits pressure built up without moving parts. Thus it has an essential advantage over other options.

It is possible in principle to push device frontiers solely by many empirical developments emphasizing components of interest. However, theoretical guidance is valuable for a reduction of the total numbers of data sets required.

An early example is the laminar heat flow mode at Zero Net Mass Flow (ZNMF). Tisza[7] argued in 1947 for a heat flow rate q proportional to the mean speed of normal fluid, proportional to the pressure gradient, Eq. (2.1), and to ρST and $(\rho s/\rho n)$; ρs is the superfluid density, ρn normal fluid density. The work of Keller and Hammel[5] and of other researchers showed that $(\rho s/\rho n)$ does not enter. It influences q however in the "supercritical" regime.

A more recent example of this nature has been VLPS work. Yuan[8] clarified important controversial points. The rate - controlling mode is flow of heat in the form of normal fluid flow in porous media separators. The recent book of Wilks and Betts[9] has documented progress in the field. Also it lists simple two-fluid equations referred to subsequently. The present report contains various sections as given in the table of contents. Appendix sections listed in the Table of Contents describe further experimental details and additional studies conducted in the present context.

3. FEP SYSTEM:

PUMP.PLUG STUDIES WITH SERIES CONNECTION OF PACKED Al_2O_3 PLUG AND Cu POWDER HEATER

There are two items:

a. Flow rate dependence on driving temperature difference;

b. Temperature profiles of the combined packed powder-heater system. (FEP runs)

The flow rate dependence work dates back to the days of near-isothermal flow investigations of Vote et al[10]. The thermomechanical rate equation has been adopted as a modified power law equation which contains recent findings concerning an "effective thermomechanical gradient". This latter version is a result of studies by Dr. Sidney Yuan et al[11]. For easy reference only the simplest cases are included here giving an example of the "1/4 power law" in each case.

The original Vote et al[10], work did not refer to the permeability of a particular flow system geometry. Instead the hydraulic diameter (D_h) of slits and ducts with circular cross section has been used. The equation is given as superfluid mean speed v_s, or as mass flow rate $\dot{m}$.

Superfluid mean speed

$$v_s = \text{const}\,[|\Delta P|/D_h]^{1/4}\,\rho^{-3/4}\,\eta_n^{1/2} \tag{3.1}$$

Mass flow rate:

$$\dot{m} = A_c\,\rho_s\,\text{Const}\,[|\Delta P|/D_h]^{1/4}\,\eta_n^{1/2}/\rho^{3/4} \tag{3.2}$$

(A_c cross section; ρ density, ∇P Pressure gradient for flow induced by external pressure difference or by gravity forces with difference $\Delta P = g\rho\,\Delta Z$; Z position). The equations appear to be "guide posts" for other cases if a switching to the thermomechanical P-gradient,

compare (Eq. 3.1) would suffice. Another convenient option appears to be the use of $L_c = \kappa^{1/2}$; (κ Darcy permeability). L_c replaces the hydraulic diameter. It is useful in particular for porous media.

An objection to the Vote et al approach is the observation that for several flow cases it is the "effective thermomechanical gradient" (∇P_T) $(\rho s/\rho n)$ which governs ∇T - induced flow.

a. Flow rate dependence on driving temperature difference

Any introduction of thermal quantities will in general cause departures from the near-isothermal resistance evolution described as power law by the Vote et al equations. The latter have, at any point of steady operation, a well-defined flow resistance. If the resistance is *above* the normal resistance or equal to it, the nature of the flow is Newtonian. There is either laminar flow or turbulent flow. The latter usually is roughness dependent. If the flow resistance is *below* the classical normal value, the system is operating on a point of the resistance transition from the superfluid to the normal flow states.

As soon as an externally applied temperature difference is switched on, the system is capable of responding with a flow rate which is not necessarily characterized by the simple arguments presented above. There are not enough data available at present to clarify this aspect of superfluid mass flow. However, the equations of Vote et al. have been modified by Yuan in order to characterize various FEP plugs. The equation incorporates the effective driving thermomechanical gradient $(\rho_s/\rho_n)\ \rho\ S\ \nabla T$. The superfluid speed and the mass flow rate are given as power law quantities for the "1/4" law as analogs of the preceding equations. Other power laws are referred to subsequently.

Superfluid velocity (mean value superficial):

$$v_s = K_4\ (|\Delta P_T|/L_c)^{1/4}\ (\rho_s / \rho_n)^{1/4}\ \rho^{-3/4}\ \eta_n^{1/2} \qquad (3.3)$$

or

$$\dot{m} = V_s \rho_s A_c = A_c \rho_s K_4 (|\Delta P_T|/L_c)^{1/4} (\rho_s / \rho_n)^{1/4} \rho^{-3/4} \eta_n^{1/2} \qquad (3.4)$$

The quantity K_4 is a constant for each pump plug as long as the power law is valid, i.e. for moderate vortex shedding rates. L_c is the square root of the Darcy permeability. Insertion of the effective gradient (eq. 3.4) permits a form of the equation quite analogous to the preceding Vote et al equation (3.1).

Mass flow rate

$$\dot{m} = \rho v A_c = \rho_s v_s A_c = K_4[|\nabla P_{eff}|]^{1/4} \eta_n^{1/2} \rho^{-3/4} \rho_s A_c \qquad (3.5)$$

The preceding equation is to be used noting that $\rho v = \rho_s v_s$, and that A_c is the total plug cross section. Pump plug data for K_4 appear to be much less dependent on the permeability than in VLPS. The pump plug results for K_4 given by Yuan et al[11] are on the order of unity for permeabilities below 10^{-10} cm^2. This implies that they are very much larger than corresponding VLPS plug constants for the same permeability.

Other power law exponents have been quoted in the literature. The most frequent number is d log m/d log ΔT = 1/3 ("derived" from the Gorter Mellink mutual friction force for zero net mass flow). For the near-isothermal transport of the Vote et al. equations, things are quite readily distinguished. The exponent d log RESISTANCE/ d log ΔP varies from unity via 3/4 to 2/3 monotonically with an increase in flow resistance. When n is converted to the exponent for mass flow versus pressure difference, we obtain m = d log v/d log ΔP = 1 - n. For instance, for n = 2/3, m will be 1/3. In contrast, the classical Blasius value is characterized by n = 4/7 = 0.5714. It is noted that the classical friction factor (f) is characterized by d log f / d log v = - 1/4. Further, d log ΔP / d log v is equal to 2 - 1/4 = 1.75 = 7/4. The value of m is 5/7 = 0.714. In other words, the classical range of power law exponents is very incompatible with the quantum liquid resistance transition under consideration.

For the thermomechanical pump plug, again the exponent m = 1/3 has been quoted. There are not enough data available for consistency checks. However, if things are similar to the resistance transition described by Vote et al., the exponent 1/3 ought to be observed for high vortex shedding rates and when the size dependence disappears as one goes from one plug to the next one in a certain pore size range. Despite the lack of data, some insight is provided by the subsequent discussion of a comparison of VLPS with ZNMF (section 5). This section 5 has the purpose of extending the plug data base into unknown regimes.

Further, for liquid transfer schemes at low ΔP, the Appendix E contains the abstract related to a paper presented at the Cryog./Eng. Conf. St. Charles IL, June 1987.

b. Temperature Profiles of the Combined Packed Powder - Heater System

This subsection reports temperature profiles of the apparatus sketched in Fig. 3.1. The Al_2O_3 portion is the FEP. It accomplishes the pressure increase associated with the application of a temperature difference ΔT. Liquid He II enters from the top flowing down into the loop and leaving at the outlet as a fountain after passing through the J-shaped stainless steel tube downstream. The packed copper section is the heater section.

The FEP tube is inside a stainless steel tube of 0.238 O.D. and 0.254 cm wall thickness. The powder is "Aluminum oxide C" of Degussa with 99.6 % Al_2O_3 and a BET surface area of 100 ± 15 m^2/g. The average primary particle size is 20 nm. The powder has been dried overnight in a vacuum oven at 125°C before compression. A stainless steel sleeve and hardened wire rams were used to compress the powder in a step-by-step procedure involving 15 compression steps. The void fraction has been about 50 % based on the density of 3.3 g/cm^3 for solid Al_2O_3.

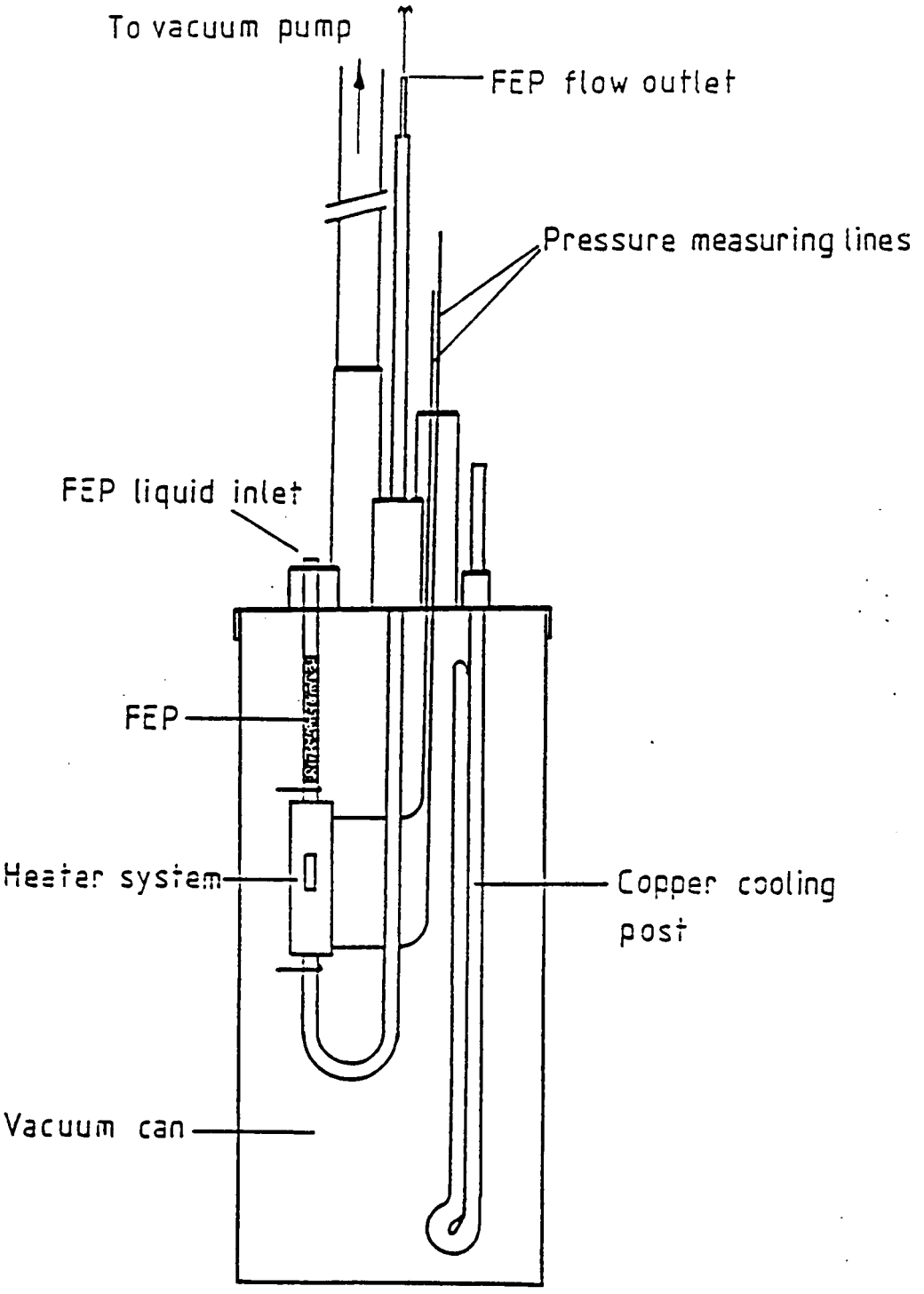

Fig. 3.1. FEP-PLUG HEATER APPARATUS
Schematic diagram of components inside vacuum can.

The copper powder system has been pressed into an OFHC copper tube (O.D. 0.635 cm, I.D. 0.335 cm, length 2.2. cm. Heater windings were made of teflon-insulated constantan wire wound bifilarly around the tube leaving room for a carbon resistance thermometer in the middle of the windings. This thermometer was mounted in a slit of 0.1 cm depth. The purpose of the Cu powder was the attainment of a large surface area permitting good contact with fluid. The powder purity is 99.2 %. The grain size distribution is listed below for different mesh sizes.

Mesh (μm)	Per cent
-325 (44)	61.6
+325 (44)	28.5
+200 (74)	9.7
+150 (105)	0.2

In a step-by-step procedure 10 layers have been applied by a press in order to achieve a relatively uniform powder packing with a void fraction of about 30%. The system may be characterized by geometry-and heat transfer-related parameters, such as the fin length based on the Kapitza heat transfer coefficient h for copper. The characteristic fin length of a simple pin fin is given by the product of the square root of cross section A_c to circumference C_c and the square root of the length k/h. The thermal conductivity is k. The fin length is written as $L_F = (K A_c / h C_c)^{1/2}$. This length has been determined as 0.06 cm at 1.8 K. The heat transfer coefficient rises with T^3. Therefore near the lambda point, the fin length is smaller, and below 1.8 K the length will become larger. Thus, there is the option of leaving a central empty core for enhanced flow, or a different coarse powder in the center for 1.8 K operation and for higher temperatures.

Temperature records are given in the next figure . They all show a flat portion and a subsequent decrease toward the bath temperature. The latter indicates "leakage" of thermal energy not utilized entirely for the thermomechanics of the FEP. Thus, termination plugs and/or different conditions of operation may be chosen.

A data sample is listed below,* and further details are given in the M.S. thesis of William Chen[12], 1987.

- - -

* App. I .

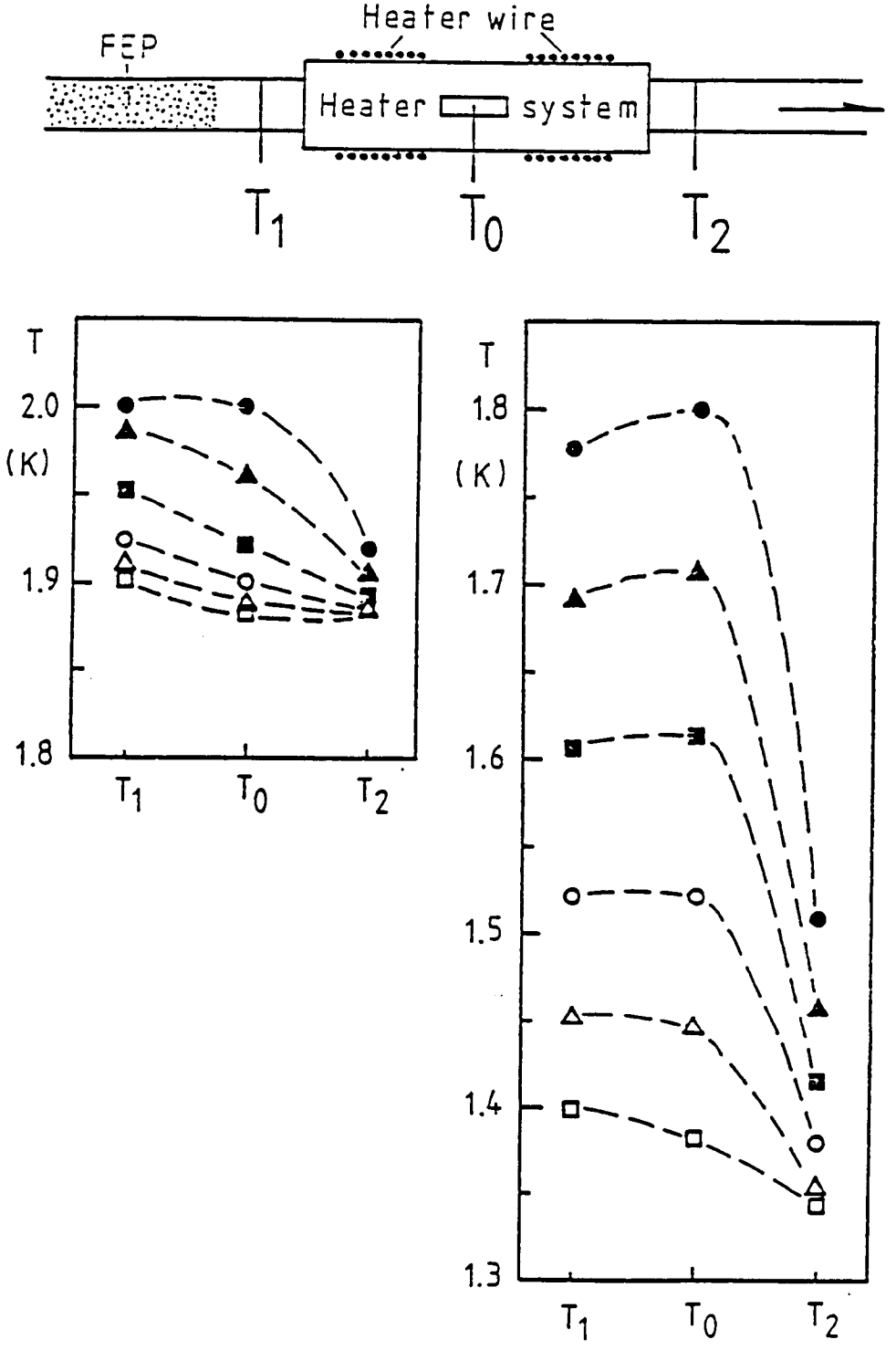

Fig. 3.2. Temperature profiles in FEP heater unit;
Left hand side : Bath near 1.9 K ;
Right hand side:Bath near 1.4 K ;
Inset : Scheme of thermometer designations;
Flow parameter example : App. F.

4. CYCLE STUDIES

The present section addresses cycles and parts of cyclic operation. The individual components in general ought to match the cycle option chosen for the entire system. In the case of the FEP, there may be a need for an aftercooler, or the liquid may be at a higher temperature without detrimental effects. For instance, in the delivery process involving a "hot" object to be cooled by He I, with associated vapor formation, there may be no need to cool fluid back to the inlet temperature of the FEP.

In several cases, the FEP may be used as "power unit" to energize other subsystems. An example is the "vortex refrigerator" (Fig 4.1) using the thermomechanics and the mechano-calorics of the He II "supereffects". The interesting point is a lack of performance figures in the literature for such a refrigeration cycle. This lack indicates a deficiency in the matching of components for specific tasks. Another point is the recognition of the role of the flow mode, e.g. resistance transition, laminar flow, roughness-dependent turbulent flow and others.

Kittel[13]quotes the "inconsistency", of the supercritical FEP , "with the usual two-fluid model". Wilks and Betts in their recent updating of the "Introduction to Liquid Helium[9]" do not go into particular details of the mechano-caloric effect. However Wilks[14] mentions in his monograph on "Liquid and Solid Helium" of 1967 that "even in the narrowest slits, the flow of superfluid will be accompanied by a flow of normal fluid". This makes it hard to accept "ideal" cases without knowing the real system behavior.

Another feature relates to vortex refrigeration based on He II thermomechanics and mechano-calorics. Tilley and Tilley[15] consider this type of refrigerator in their first edition. However the second edition of their book omits the refrigerator. One may see this as an indication of a lack of interest or of knowledge or both. Most likely, very few cryocooler special-

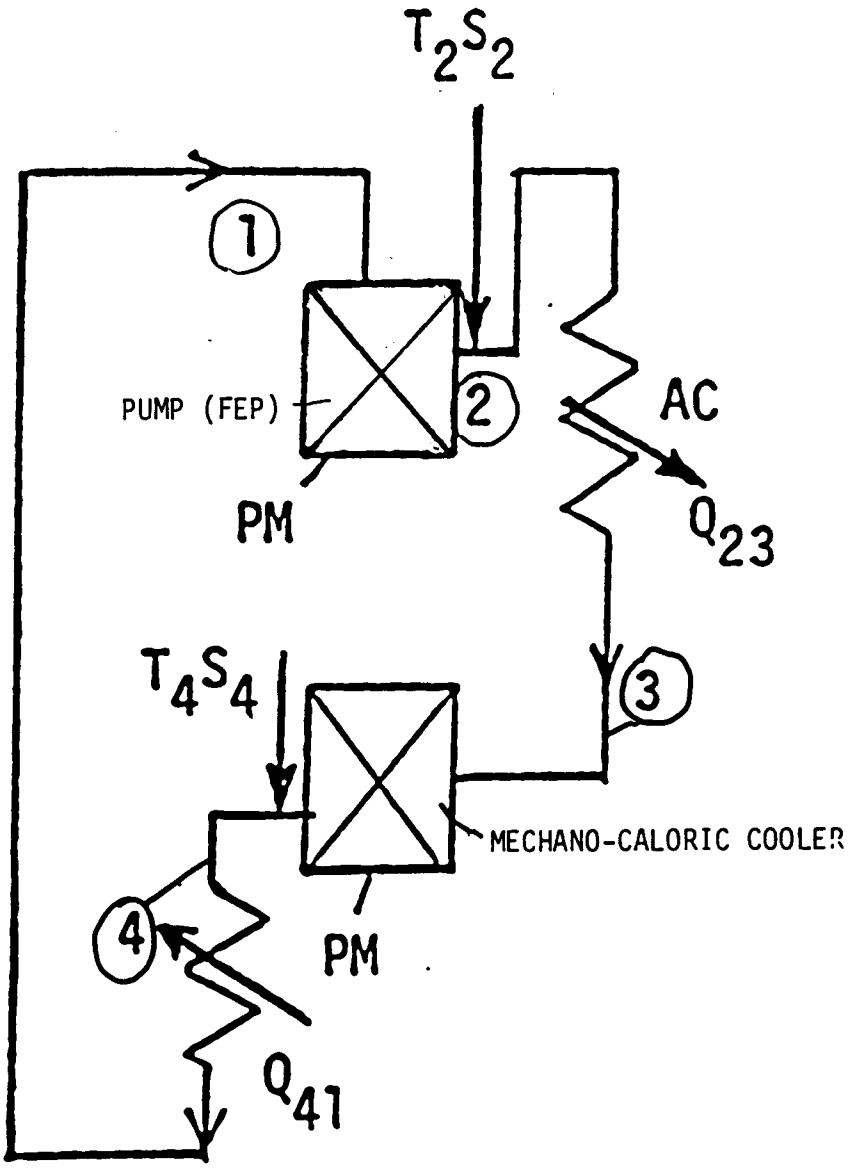

Fig. 4.1. VORTEX REFRIGERATOR , schematically
AC AFTERCOOLER ; PM POROUS MEDIUM

ists have taken notice of the He II vortex refrigeration option.

Once thermodynamic changes of state are introduced as ideal changes, there is always a question about non-ideal conditions and tayloring of optimized components for a special task. As usual there appear to be different options, and each task has certain constraints implying a lack of generality when applied to another problem. Therefore, the following simplified statements are to be considered with some caution as experimental data are quite scarce. With these precautions in mind, cycle results are given in simplified form for the ideal μ-P-μ-P cycle and for the corresponding cycle with counterflow heat exchanger prior to the refrigeration stage. The system is shown schematically in Fig. 4.1.

The cycle designation is based on constant parameter references. The initial state change $d\mu = 0$, or $\mu = \text{const}$, designates constant chemical potential. The pressure is raised in an ideal manner, as described by London's equation. In the second state change, isobaric cooling is achieved. The third state change implies constant chemical potential with a depressurization. This state change leads to cooling. Ideally, the decrease in temperature is given by

$$(\partial T/\partial P)_{\mu} = 1/(\rho S) \tag{4.1}$$

Afterwards, thermal energy is picked up isobarically. From the point of view of classical heat exchanger operation, isobaric assumptions apparently do not present very challenging tasks. However, the T-profiles of section 3 provide hints about design constraints. different case. Further, there is nearly no quantification at all for the real depressurization process at $d\mu = 0$.

The effectiveness results appear to throw some light on the refrigeration process. Initial motivation for the vortex refrigerator introduced by Staas and Severijns (compare also App. A), appears to have been related to attainment of low temperatures. Obviously, the theroretical calculations based on ideal liquid do omit the lattice contributions of the real

"superleak" plug which provides the cooling. The refrigeration capability is elucidated by a brief look at the opposite *direction* i.e. a power cycle. Very little power is gained as the area enclosed by the cycle in a pressure-volume diagram is extremely small. This feature relates to the small volume changes in liquids. Thus, there are very few attractive points for power cycle operation. However the opposite appears to be true for refrigerator operation. Very little work is needed for heat pumping in view of the small volume changes. Moreover, the use of parasitic heat is a very attractive feature. It is near at hand to omit system *preparation* for a first look. Thus, the usual environmental temperature of about 300 K has been disregarded completely, (as in similar analysis of the fountain effect pump thermodynamics). The definition used for the COP (= coefficient of performance) is the ratio of heat pumped to heat input. This COP ideally is

$$COP = T\ S\ /Q_R \tag{4.2}$$

The simplest case is a refrigeration load

$$Q_R = T_4\ S_4 + |Q_{41}| \tag{4.3}$$

Assumed is the sequence 1-2 for $d\mu = 0$ and so on. The system's thermodynamic path is shown schematically in the T-S diagram, Fig. 4.2. The coefficient of performance (COP) is depicted in Fig. 4.3. It is seen that reasonable values of COP are reached at relatively high bath temperature T_1, for a specified pressure difference. Fig. 4.4 shows the cold end temperature versus T_2.

The effect of a *counterflow heat exchanger* (Fig. 4.5) is known from classical systems. The COP usually is lowered, if all other parameters are kept constant, and the heat exchanger covers a specified temperature difference prior to the refrigeration stage. The final temperature is decreased for such a system, and the compensation of a drop in COP is possible in priciple using a lower ΔP in the FEP. Figure 4.5 presents designations for the cycle with

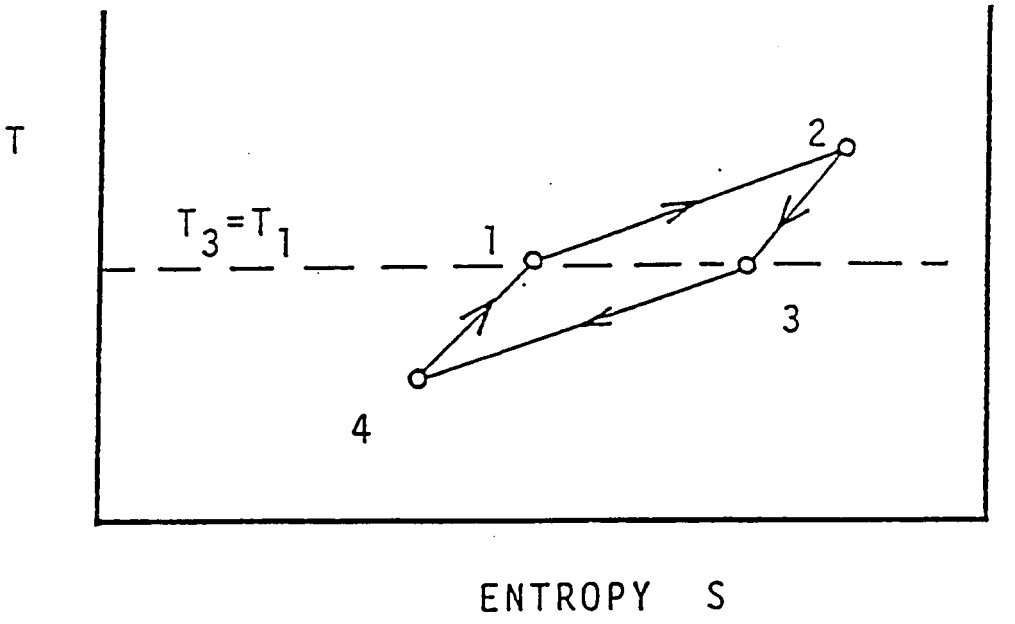

Fig. 4.2. TEMPERATURE-ENTROPY DIAGRAM

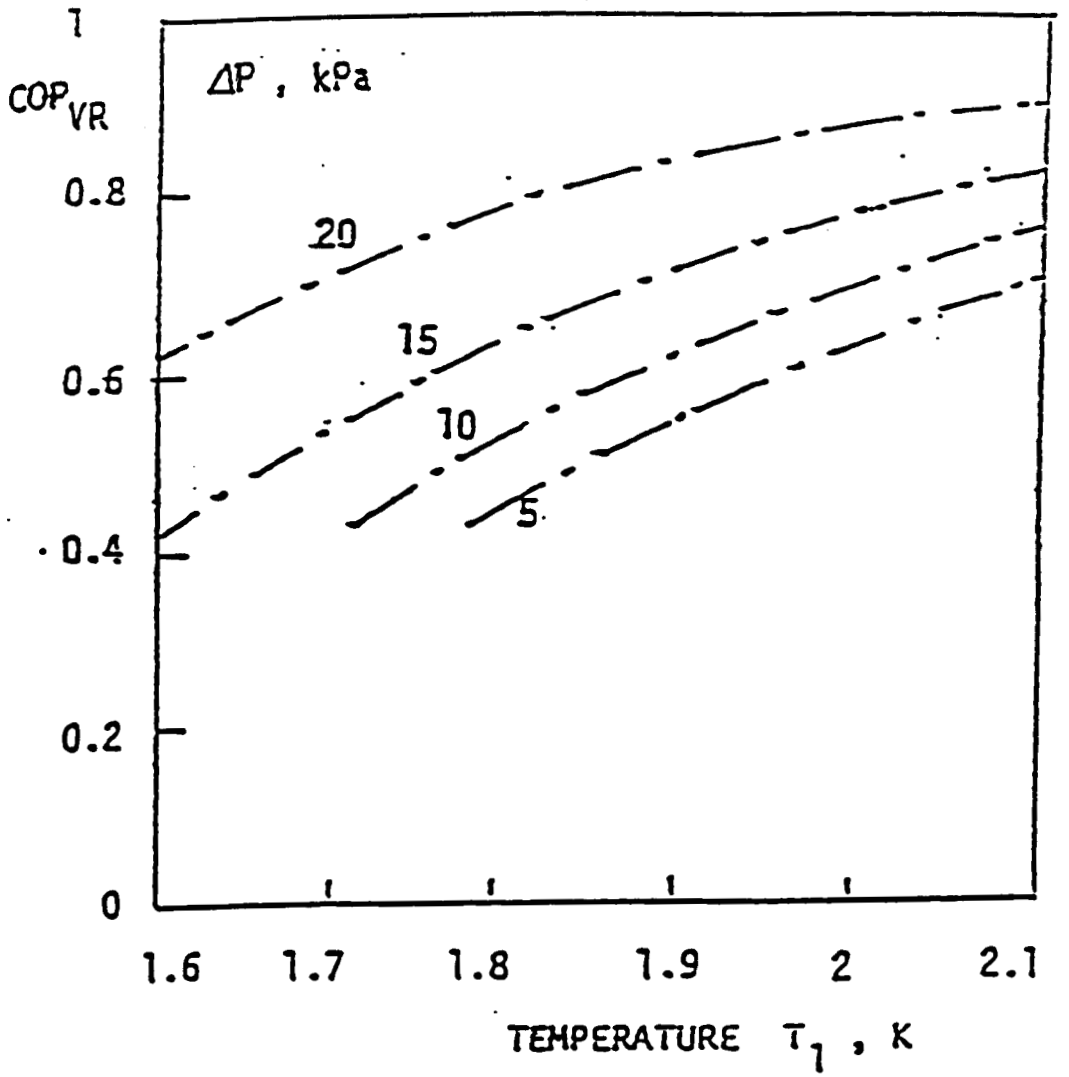

Fig. 4.3. COEFFICIENT OF PERFORMANCE $(COP)_{VR}$ OF VORTEX REFRIGERATOR VERSUS INITIAL TEMPERATURE T_1

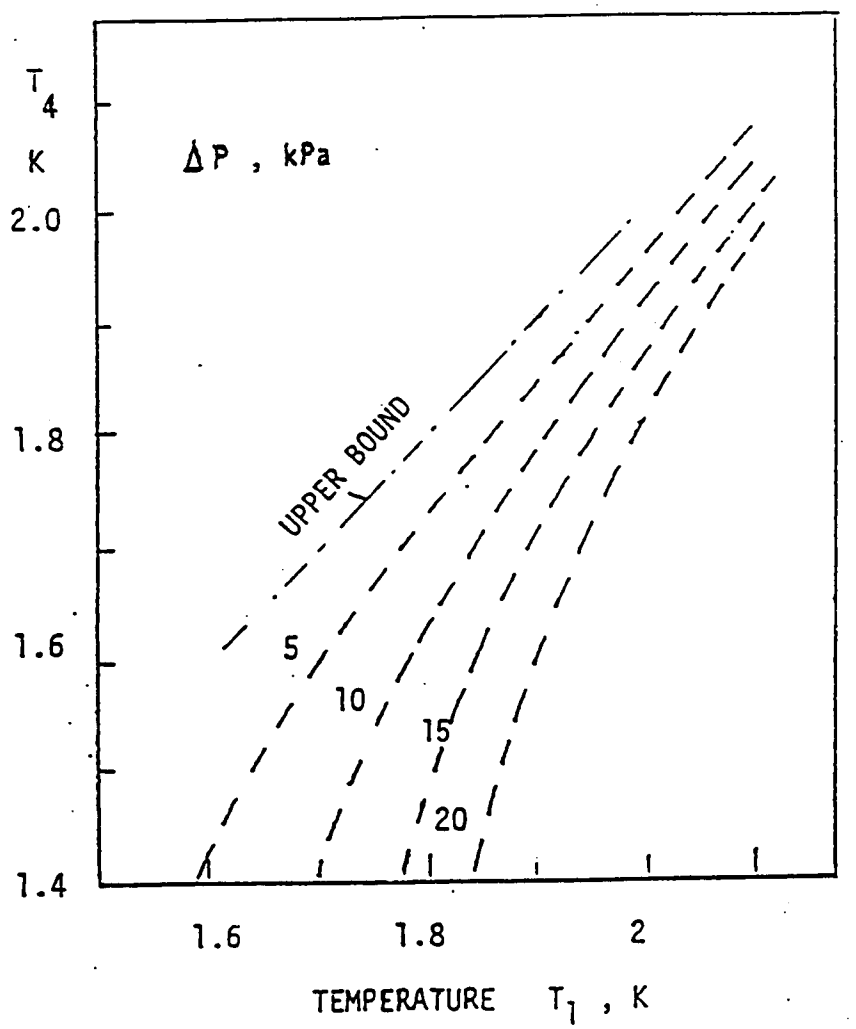

Fig.4.4. Ideal cold end temperature T_4 achieved in the μ–P–μ–P VR cycle, versus initial temperature T_1 ("bath temperature"), for various pressure increases in the fountain effect pump (ideal FEP)

precooling by counterflow heat exchange. Fig. 4.6 depicts the system. Fig. 4.7. shows the COP results and cold end temperatures for a parametric study with the precooling temperature ratio as parameter. A relatively small effect of precooling appears to provide considerable modifications of the ideal system performance. The parametric studies have been conducted for a pressure difference of 100 milli-bar. In the limit of a temperature ratio of unity, the previous simple cycle μ-P-μ-P is recovered.

Real component selection has to consider two items in each plug for ideally constant chemical potential. One case is the porous media selection for the specifications. The other case is the heat absorption/heat rejection unit optimization. In addition there are connecting plumbing devices and controls. The simple wide tube connection appears to be a low flow resistance solution. As shown by the FEP duct data however, there is a good chance of heat flow by counterflow action. Fortunately, there is a very small slip of normal fluid and superfluid at high mass flow Reynolds numbers. This implies a possible need for balancing of slip versus pressure drop in a real refregerator. Another solution is the use of "pressure relieved mass transport" using porous media coatings (wick-like structures) for wall coverage. There appears to be very little information available in this area.

In summary, the vortex refrigerator has an attractive potential for He II - cooled systems and subsystems, however considerable R & D work is required for general acceptability. This includes the interfacing between He I portions and He II subsystems during system preparation. Nevertheless, there are very advantageous features indicated by the present calculations which pint out good performance when T is not too low, e.g. near 1.8 K to 2 K.

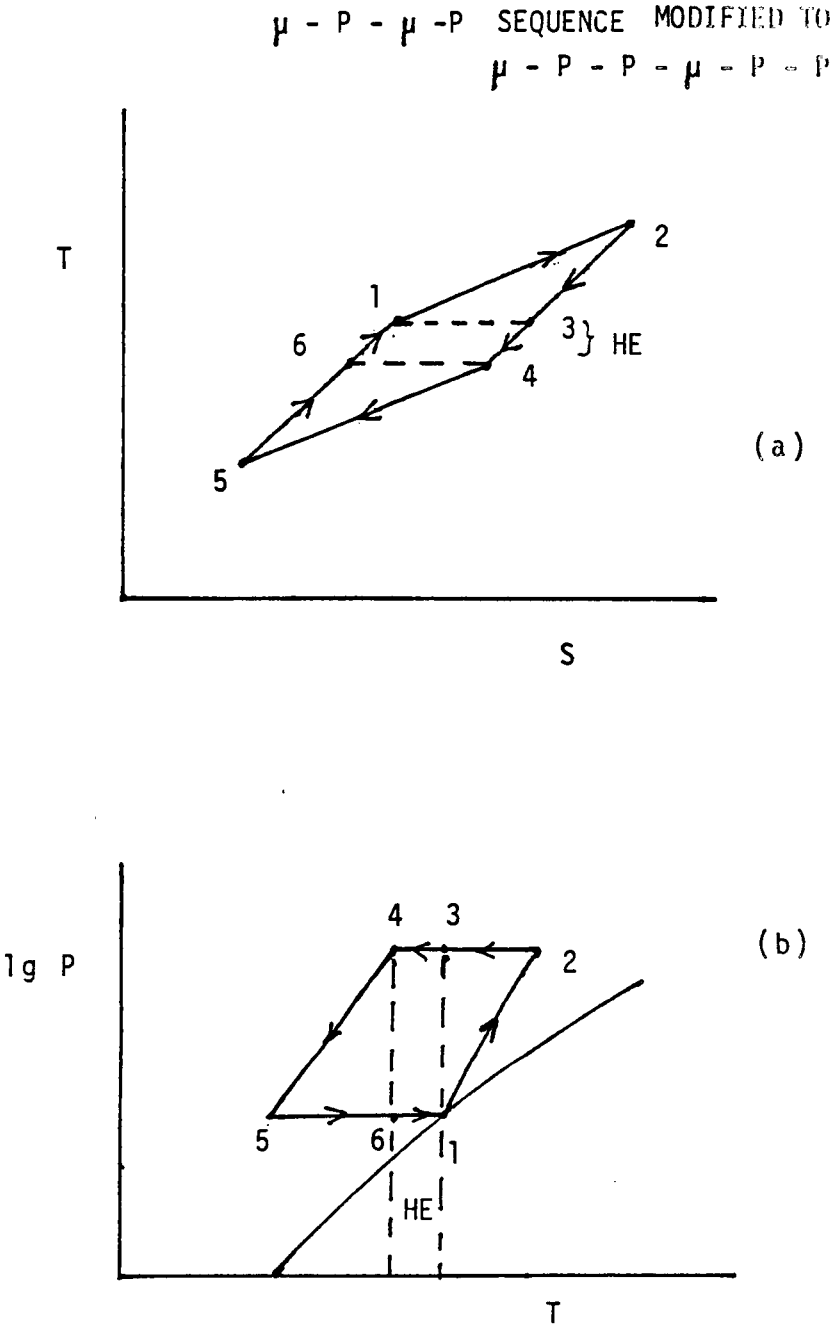

FIGURE 4.5. Schematic diagram of cycle with counterflow HEAT EXCHANGER (HE) a. T-S diagram, schematically, log-log coordinates;

b. log P versus T diagram, schematically; point 1 is on the saturated vapor-liquid equilibrium curve.

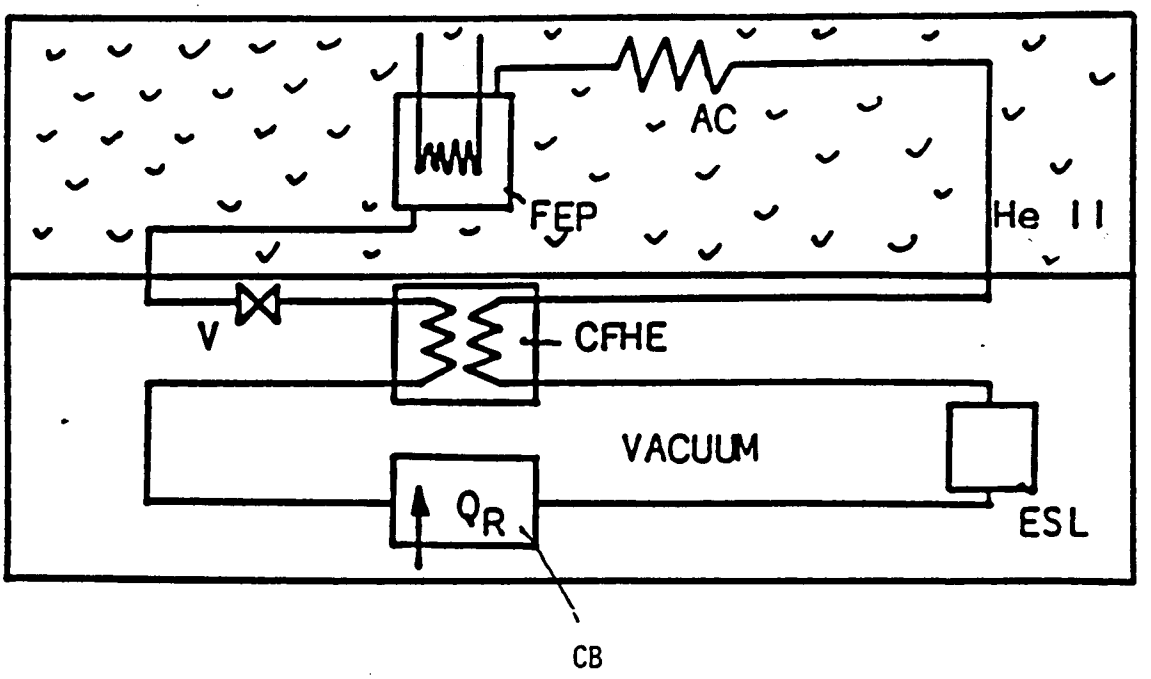

Fig. 4.6 . VORTEX REFRIGERATOR WITH COUNTERFLOW HEAT EXCHANGER (CFHE), schematically;
AC AFTERCOOLER
CB COLD BOX
ESL "EXPANSION SUPERLEAK" = MECHANO-CALORIC UNIT
FEP FOUNTAIN EFFECT PUMP WITH HEATER ACTIVATION
V VALVE

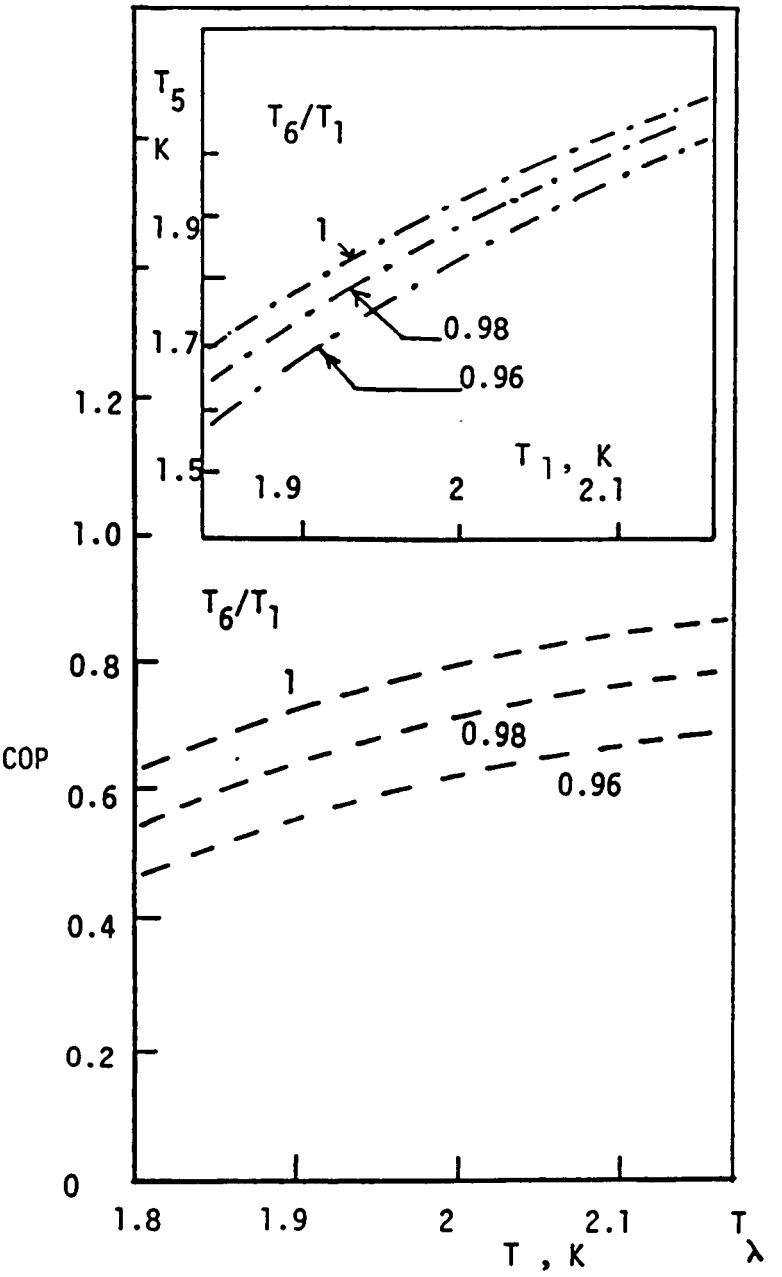

Fig. 4.7. COP FOR CYCLE WITH IDEAL HEAT EXCHANGE ; INSET : COLD END TEMPERATURE VS T_1 .

5. POROUS MEDIA TRANSPORT CHARACTERISTICS

The experiments have included basic studies of vortex shedding processes during heat flow in porous media. In conjunction with the power law fits for FEP pump plug data, the determination of the rate of mass/superflow versus applied temperature difference has been a major goal of the present work. However, from literature the most common case of Zero Net Mass Flow (ZNMF) been found to be pursued only in a limited range. In particular the large ΔT-range (non-linear range) has received but little attention. Therefore, this part of the studies has aimed at an extension of heat transport knowledge, available previously from VLPS work.

The experiments have used plugs whose axis has been oriented in vertical direction. Heat flow has been directed in the "g" direction downward. Heating has been initiated using step inputs in heating power. Heater windings have been mounted in an insulated chamber. The step input in power in general produces the following events:

1. At low power, a nearly exponential first order change with a temperature difference ΔT proportional to $[1 - \exp(-t/\tau)]$ is observed; τ = characteristic time; t = time.

2. At a certain power, linearity is destroyed. The final value observed at long time is considered the result of quasi-steady operation. The q versus final ΔT curves are non-linear.

3. Above a moderate power, there is no chance to reach a well-defined quasi-steady heating condition at long times. Instead, at an intermediate time, there is a drop in ΔT as a result of vapor formation.

4. Near the onset of case 3, there is a finite chance for large amplitude, slow, non-linear oscillations.

Figure 5.1 is a schematic drawing of the setup. Figure 5.2. presents a thermogram example. Figure 5.3 is a similar example with oscillations. Fig. 5.4. displays the results, at long times of quasi-steady linear and non-linear conditions.

Figure 5.4 shows a linear region given by the permeability of the plug. The analog of Darcy's law is used.

$$q_o = \rho\ S\ T\ v_{no} \tag{5.1}$$

with a superficial normal fluid velocity of

$$v_{no} = \kappa_n\ |\nabla\ P_T|/\eta_n \tag{5.2}$$

The normal fluid permeability is κ_n. The grad P_T - term in Equation (5.2) is the London pressure gradient of the thermomechanics of He II.

Figure 5.5. shows permeabilities obtained as a function of temperature for plug PK -K-10-S-02- 6.4 x 0.75

The interpretation of the linear regime is straightforward noting that the small ΔT of that range does not present difficulties of property definitions.

In the non-linear regime things are less straight forward. A procedure has been used initially in parallel to phase separator (VLPS) work. The simple modified plug equation incorporaties a size-dependent (dimensionless) plug constant k^*_{ZNMF}. The equation is semi-empirical because of the implications of power law exponents discussed above in the preceding section. The simple analog of VLPS is given as superficial heat flux density q.

$$q = K^*_{ZNMF}\ \rho s\ S\ \ T\ \ [(\rho_s/\rho_n)\,|\nabla\ P_T|\ (\eta_n/\rho)]^{1/3} \tag{5.3}$$

Results for the plug PK-K-10-S-02-6.4 x 0.75 are shown in Figure 5.6.

Details of related numerical work are given in the Appendix Sections D and E.

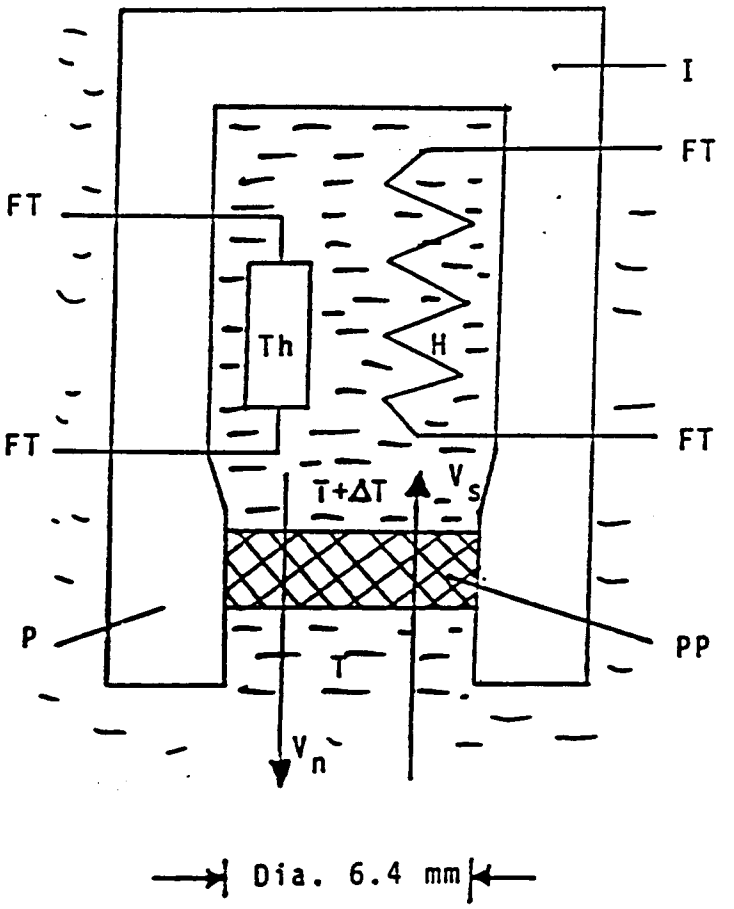

Schematic diagram of porous plug

Th- Thermometer, H- Heater, PP- porous plug
P- phenolic, FT- Feed Through
I - Insulation

Fig. 5.1. Schematic diagram of experimental system for zero net mass flow (ZNMF) ; piug of PK series.

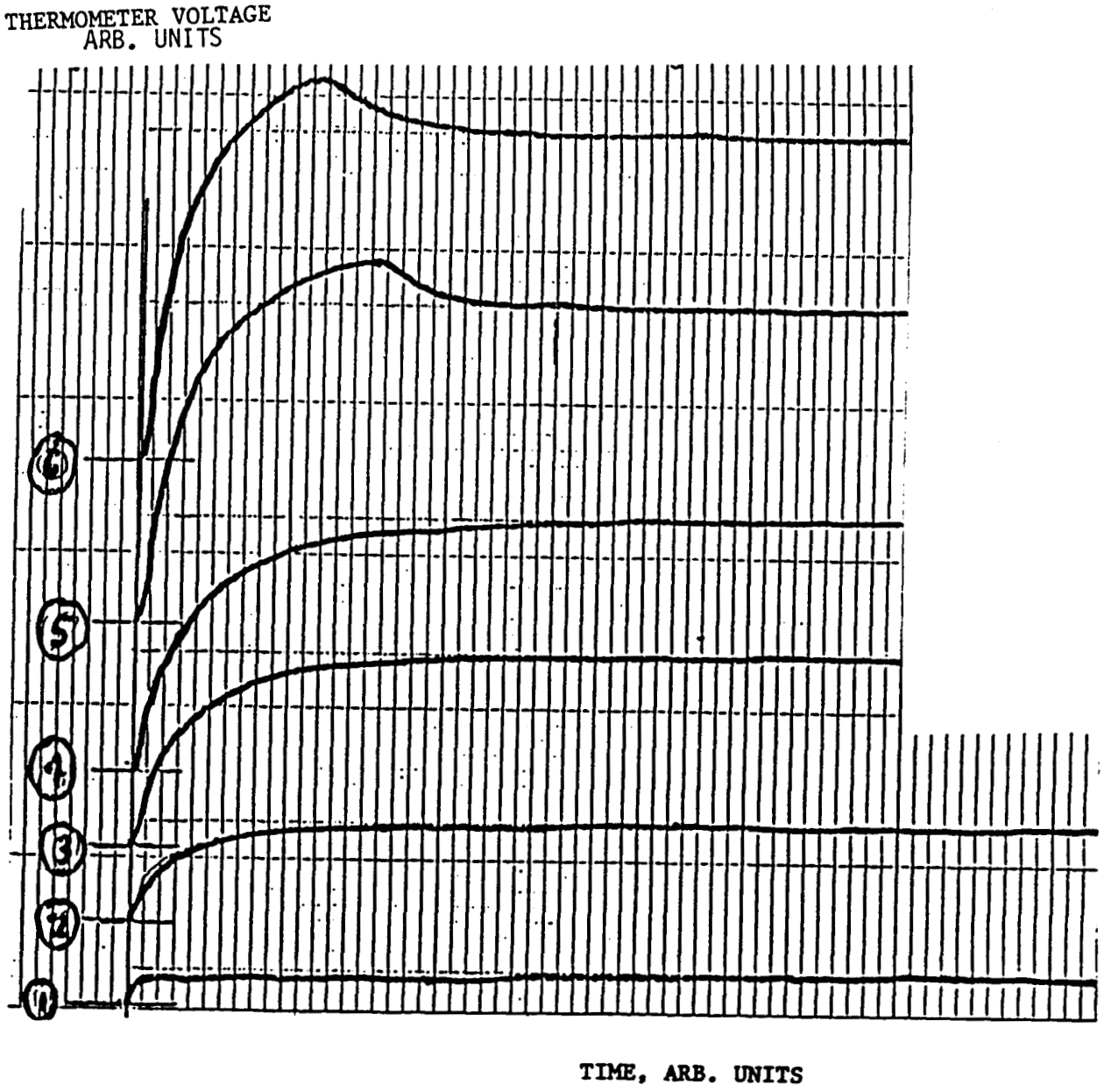

Fig. 5.2 THERMOGRAM EXAMPLE : PARAMETER : HEATER CURRENT

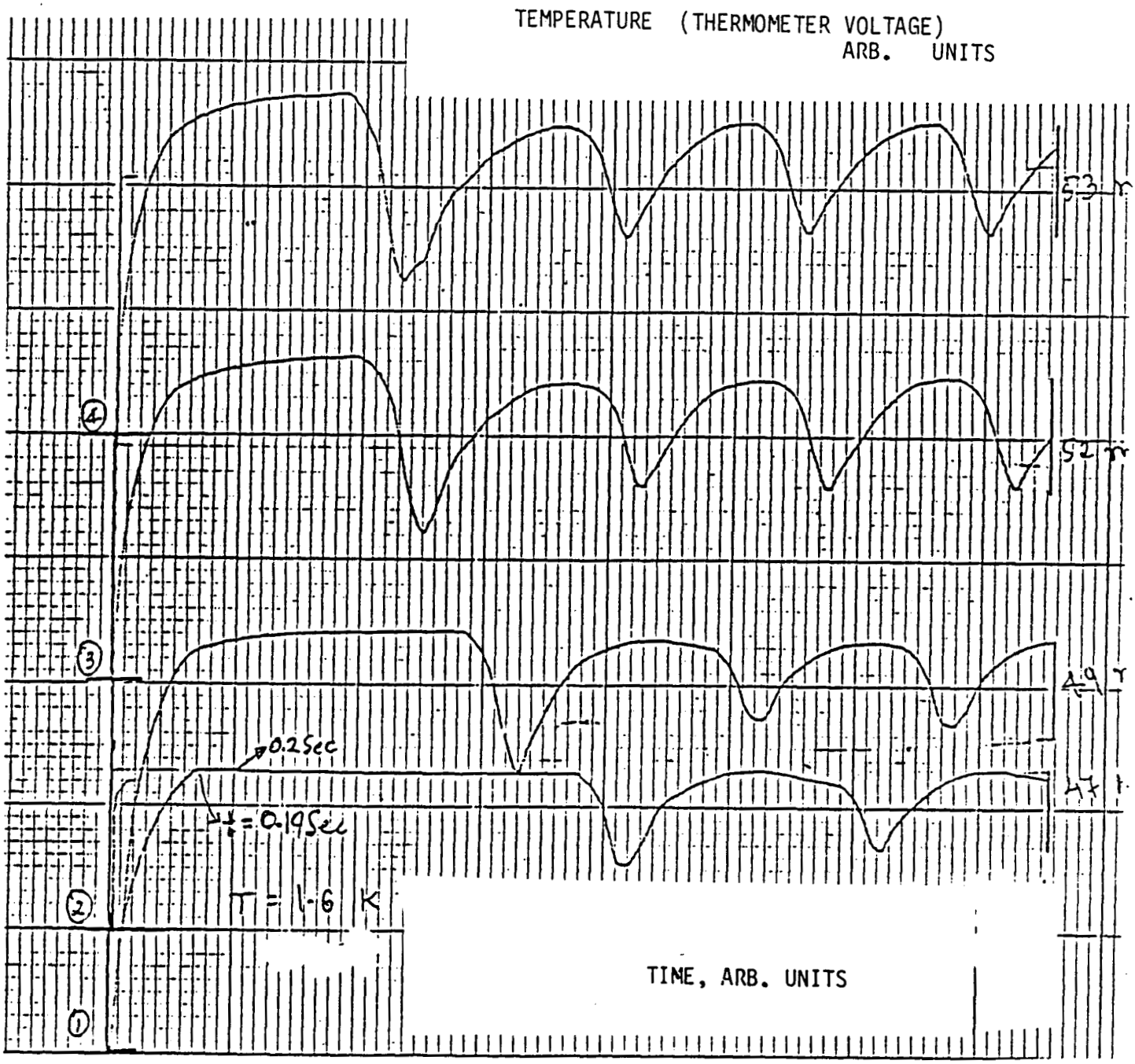

Fig. 5.3. THERMOGRAM EXAMPLES INCLUDING OSCILLATIONS

Eqs. MOTION – 2-FLUID MODEL , truncated,
WILKS – BETTS , op. cit.

$$\partial \vec{v}_s / \partial t = S \text{ grad } T - (1/\rho) \text{ grad } P$$

$$\partial \vec{v}_n / \partial t = -(\rho_s / \rho_n) S \text{ grad } T - (1/\rho) \text{ grad } P$$

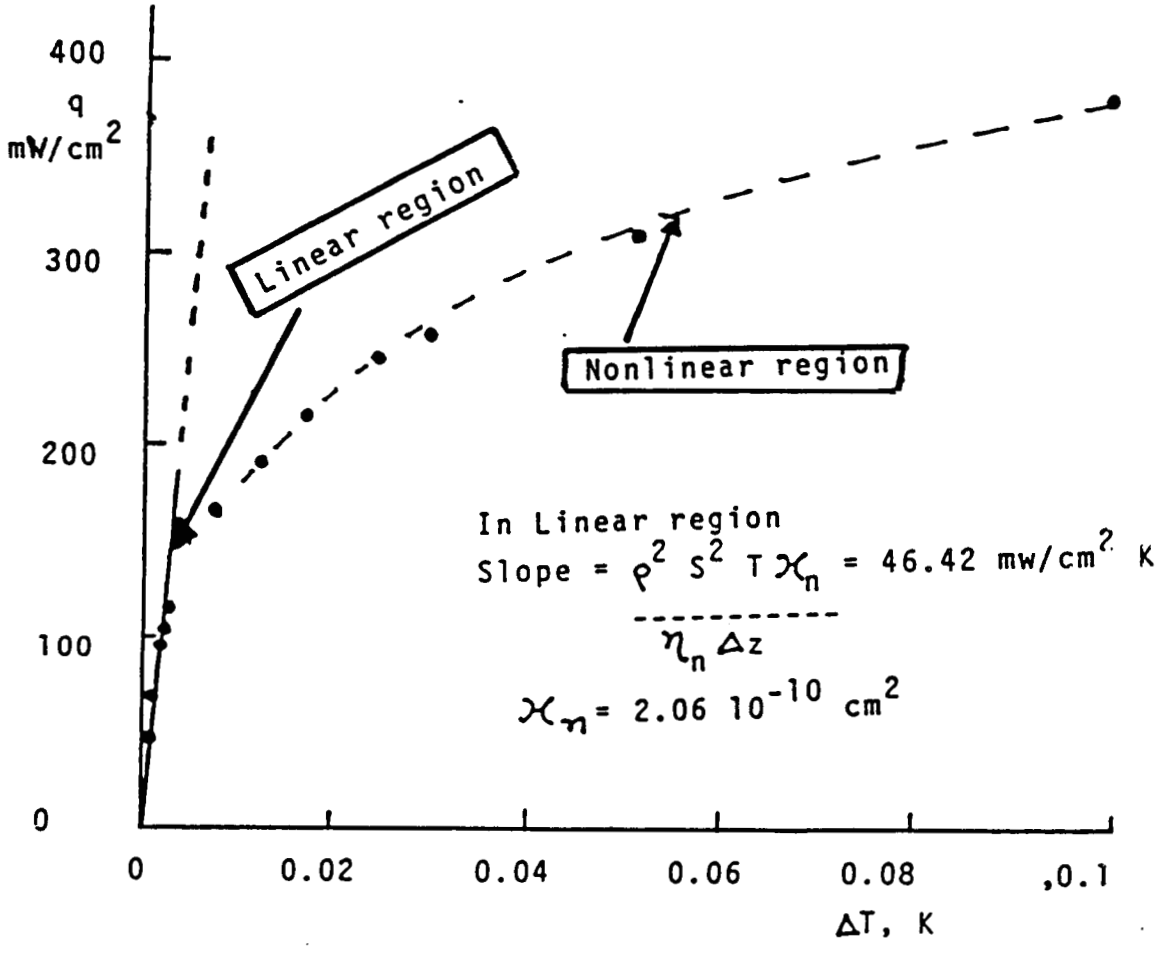

FIGURE 5.4 Heater power q vs ΔT at bath temperature near 1.9 K.
Inset : TWO-FLUID EQUATIONS .

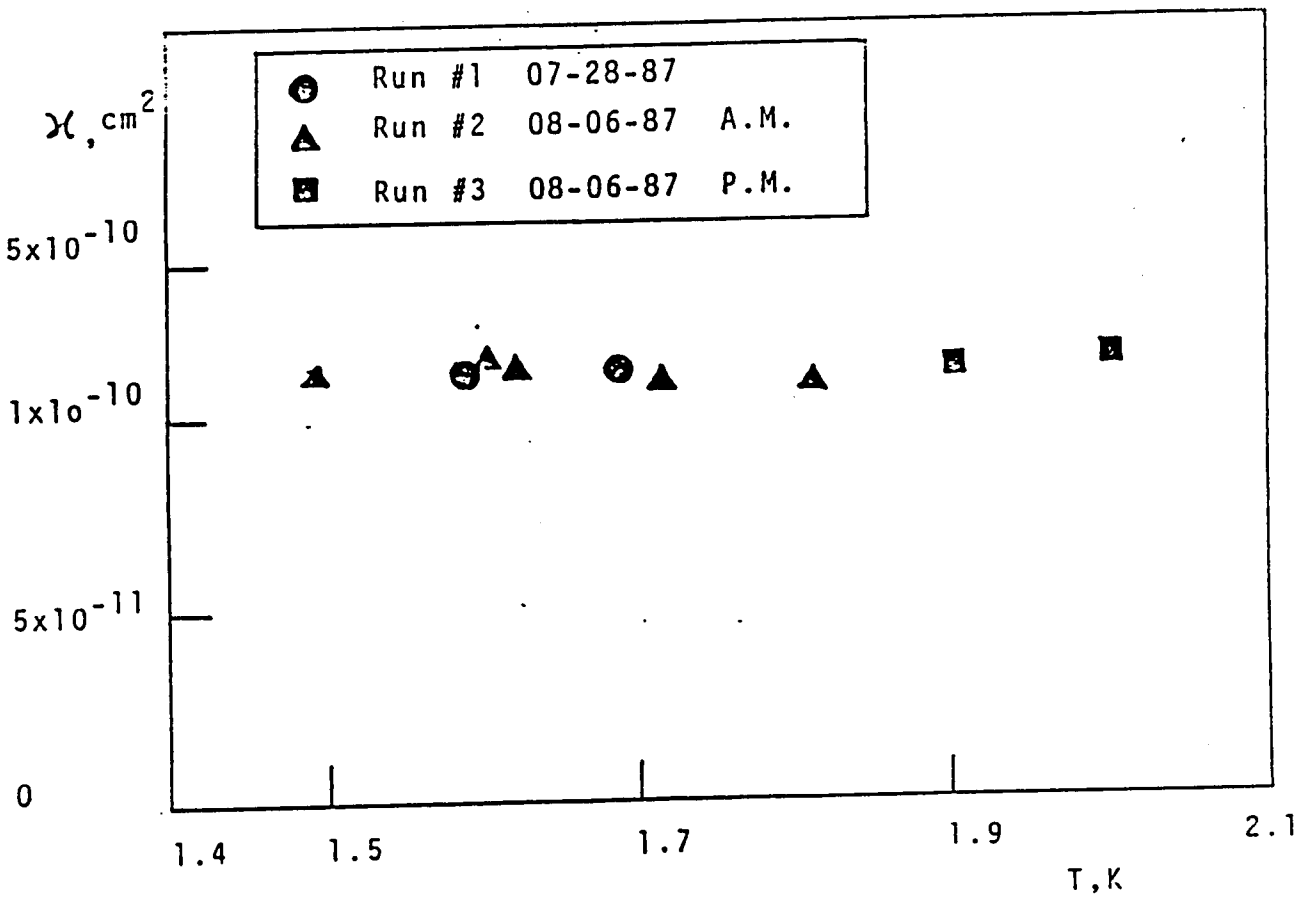

Fig. 5.5. DARCY PERMEABILITIES VERSUS T .

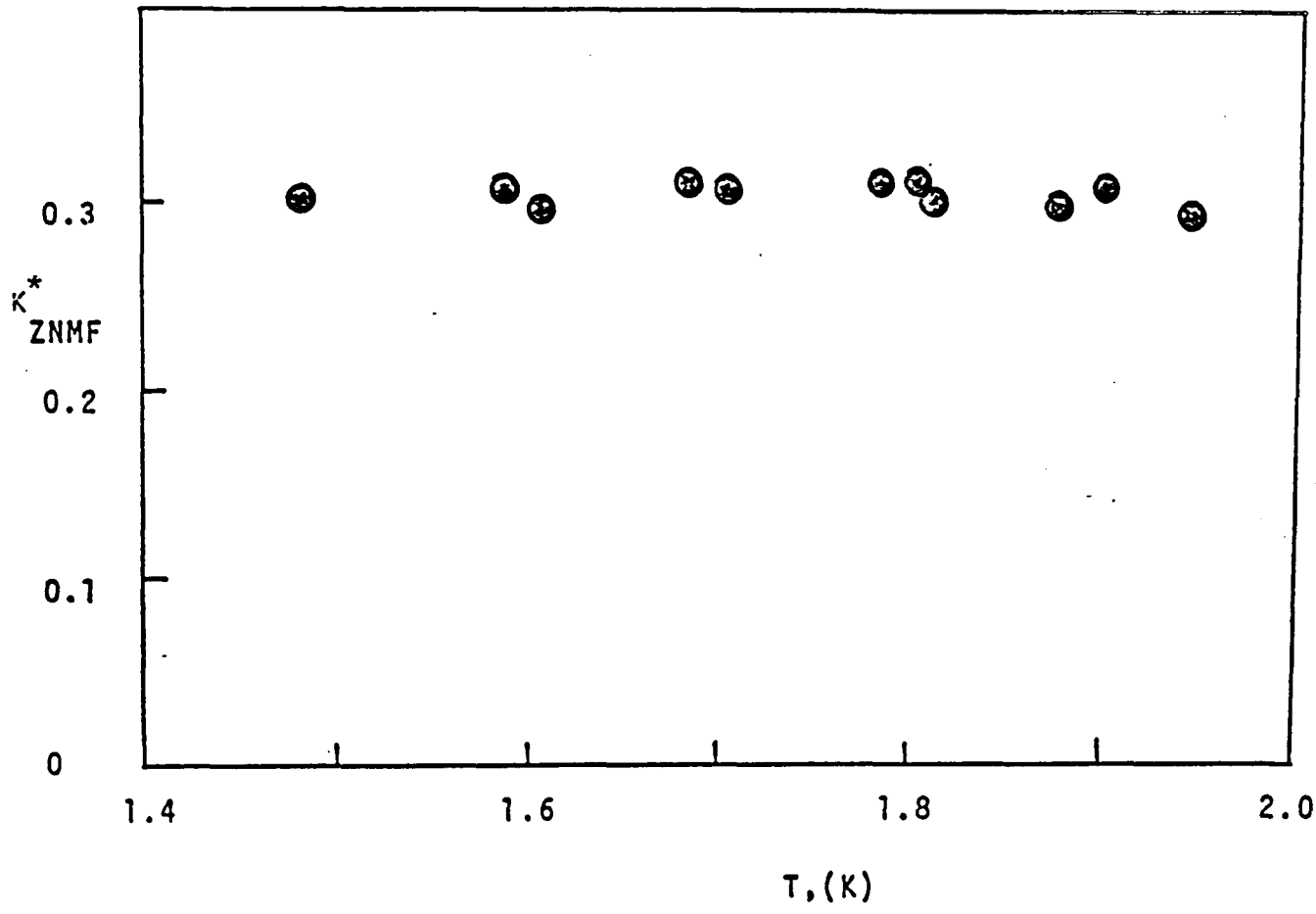

Fig. 5.6. Rate constant K^*_{ZNMF} as a function of bath temperature.

The change to a more meaningful power law exponent involves a characteristic length. For instance, the case of an exponent of 1/4 is quite significant. There is a characteristic length involved in the interaction of pore walls with fluid motion. Appendix E presents details of this approach. In the course of the work, the data obtained indicate that the constants replacing K^*_{ZNMF} in Equation 5.3 retain the size dependence qualitatively.

In phase separator (VLPS) plugs the size dependence is at variance with ZNMF in so far as data appear to be numerically above the VLPS plug equation. However the data trends of the constants of Eq. 5.3 are retained. A comparison is available using Figures 5.7 and 5.8.

In summary, it is seen that early indications of transport phenomena in plugs are confirmed. Jeffrey M. Lee had already indicated in his M.S. thesis (UCLA 1983) that certain plugs pointed in this direction. The VLPS results of Yuan's Ph.D. thesis (UCLA 1985) put this suspicion on a firm footing in the VLPS area. The data obtained so far for ZNMF appear to confirm the trend of the VLPS data also for ZNMF. Thus, the peculiarities of FEP units are in considerable contrast to the conditions of VLPS and ZNMF modes.

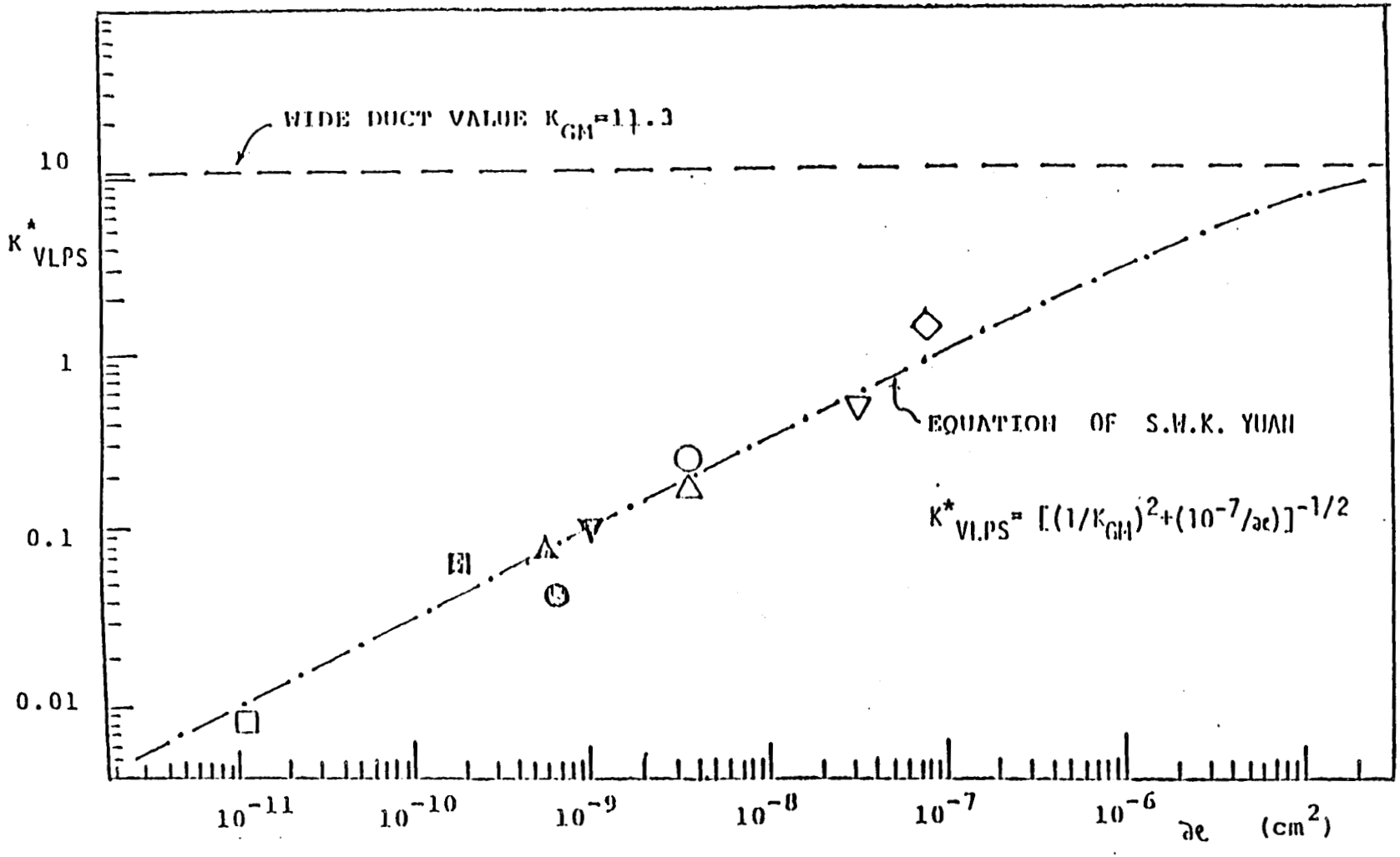

Fig. 5.7 POROUS MEDIA RATE CONSTANTS OF PHASE SEPARATOR PLUGS VERSUS PERMEABILITY

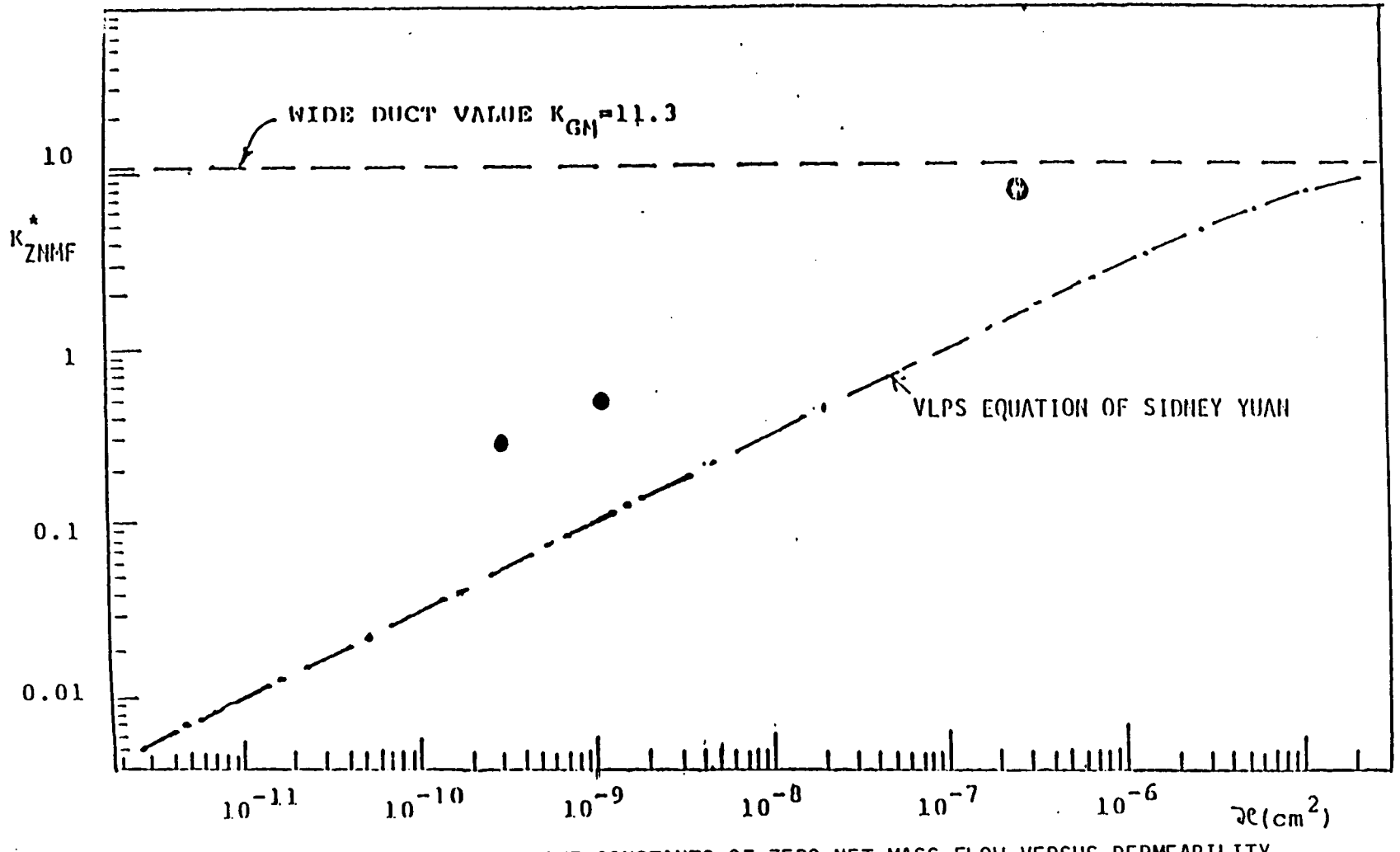

FIG. 5. 8. POROUS MEDIA RATE CONSTANTS OF ZERO NET MASS FLOW VERSUS PERMEABILITY

6. SUMMARY INCLUDING COUNTERFLOW COOLING OF COMPONENTS

Studies of fountain effect-induced phenomena and system options have been continued with the goal of improved fluid management starting near 2 K. Instead of looking at fluid management only from the point of view of routing "hot" to "cold" production lines, the alternate scheme of managing from "bottom" to "top" is suggested by the He II work involving local He I domains. For instance, solid hydrogen pellets may be carried hydraulically instead of pneumatically on the basis of the Low-T cryogenic fluid.

The porous plug results are an important data set for various thermomechanical modes. A temperature difference is not possible unless the porous medium restricts the cross section to suppress the flow of normal fluid. The permeability range covered in the present runs has been reduced from the previous phase separator range to the order 10^{-10} cm^2. The phase separator modes of previous work have been compared to the data sets for zero net mass flow (ZNMF). The ZNMF data do indeed follow phase separator plug trends. The absolute ZNMF transport rates obtained however are quantitatively higher than the phase separator data.

The extension of the work to He II vortex refrigeration has been based on the preceding calculations of FEP units. The addition of the mechano-caloric plugs presents a novel component set to be quantified in transport details for the purposes of refrigeration and heat pumping. Previous vortex refrigerator work appears to have been motivated primarily by attainment of the lowest possible temperatures. The performance figures appear to be a special class among various cryocooler systems. The COP values are attractive for operation near 2 K i.e. in the upper T range of He II, and not in the lower one.

Finally, there is an interesting implication for "lifetime extension". The usual space vessel of the IRAS type has the VLPS location set rather far away from heat input locations.

This approach appears to be advisable for the understanding of the mode of operation prior to more sophistication. With the success of IRAS however, the question for improvements includes the use of the VLPS effect and TM effect in order to intercept certain heat inputs. If less heat arrives at the bath, the vaporization rate is reduced and the He II is kept in the vessel for a longer period of time. Another point is the incorporation of the vortex refrigerator into this type of concept for improved fluid management of the future.

7. REFERENCES

1. Allen, J.F. and Jones, H. *Nature* 141, 243, 1938.
2. Kapitza P.L., *Nature* 141, 74, 1938.
3. Allen, J.F. and Misener, A.D., *Nature* 141, 75, 1938.
4. Keller, W.E. and Hammel E.F., *Ann. Phys.* 10, 202, 1960.
5. London, F. *Superfluids,* Vol. 2, Wiley, New York 1954.
6. Severijns, A.P., *Cryogenics* 20, 115, 1980.
7. Tisza, L., *Phys. Rev.,* 1947.
8. Yuan, S.W.K., *Ph.D. thesis, UCLA,* 1985.
9. Wilks, J. and Betts, D.S. *An Introduction to Liquid Helium,* 2nd Ed. Oxford Univ. Press, 1987
10. Vote F.C. et al., *Adv. Cryog. Eng.* 16, 393, 1971.
11. Yuan S.W.K. and Nast T.C., *Cryog. Eng. Conf.* St. Charles IL, 1987 paper BC-4.
12. Chen, W.E.W., *M.S. thesis, UCLA* 1987.
13. Kittel P., *Cryogenics,* 27, 81, 1987.
14. Wilks, J. *Liquid and Solid Helium,* Oxford, Clarendon, 1987.
15. Tilley D.R. and Tilley, J., *Superfluidity and Superconductivity,* Wiley New York, 1974.
16. Staas, F.A. and Severijns, A.P., *Cryogenics,* 9, 422, 1969.

APPENDIX B: Vortex Shedding Regime in Porous Media: Modified Mutual Friction Transport Regime of Counterflow

It is noted that porous media transport is not the usual mutual friction transport proposed by Gorter-Mellink. However, for an assessment of the special porous plug conditions, the frame of reference of Gorter-Mellink provides insight and empirical equations for VLPS design. First, vapor liquid phase separation (VLPS) is discussed. Second, zero net mass flow (ZNMF) is treated.

Consider VLPS modes in the form proposed by S. W. K. Yuan. The rate constant K* = K^*_{VLPS} is contained in the equation for the superficial mass flux density (= mass flow rate per total plug cross section divided by the density).

$$\bar{j}_o = K^*_{VLPS}[\lambda+ST]^{-1}\rho_s ST[(\rho_s/\rho)S(dT/dz](\eta_n/\rho)]^{1/3} \tag{B.1}$$

In general, Eq. (B.1) has to be integrated in order to take the T-dependence of properties into account. Details have been given in the Ph.D. thesis of Dr. Sidney Yuan.

The related equation for the heat flux density associated with the mass flux density is given by $\bar{q}_o = \lambda\bar{j}_o$, or

$$(\bar{q}_o)_{VLPS} = K^*_{VLPS}\lambda[\lambda+ST]^{-1}\rho_s ST[S\,|\nabla T|(\rho_s/\rho_n)(\eta_n/\rho)]^{1/3} \tag{B.2}$$

For finite temperature differences, Eq. (B.2) is integrated for steady transport: $\int\bar{q}_o^3 dz = K^*_{VLPS}\int f(T)dT$, or

$$(\bar{q}_o)_{VLPS} = K^*_{VLPS}(L)^{-1/3}\left\{\int\lambda^3(\lambda+ST)^3(\rho_s ST)^3 S(\rho_s/\rho_n)(\eta_n/\rho)dT\right\}^{1/3} \tag{B.3}$$

For the linear regime (Appendix C), the relationship between VLPS and ZNMF is:

$$(\bar{q}_o)_{VLPS} = (\bar{q}_o)_{ZNMF}/(1+ST/\lambda) \tag{B.4}$$

Using Eq. (B.4) for ZNMF results in the following:

$$(\overline{q}_o)_{ZNMF} = K^*_{ZNMF}\rho_s ST[(\eta_n/\rho)(\rho_s/\rho_n)(S\Delta T/\Delta z)]^{1/3} \quad ; \quad \Delta T \ll T \tag{B.5}$$

($\Delta z = L$).

Again the case of large ΔT necessitates integration due to the strong temperature dependence of the properties $\rho_s(T)$ and $S(T)$. By grouping all temperature dependent properties into one term F(T), Eq. (B.5) becomes:

$$(\overline{q}_o)_{ZNMF} = K^*_{ZNMF}[F(T)\nabla T]^{1/3} \tag{B.6}$$

The property function is

$$F(T) = \rho_s^4 S^4 T^3 \eta_n/(\rho_n \rho) \tag{B.7}$$

Integration leads to

$$\int_{z=0}^{z=L} (\overline{q}_o)^3_{ZNMF} dz = K^{*3}_{ZNMF} \int_{T}^{T+\Delta T} F(T)dT \tag{B.8}$$

The result is

$$(\overline{q}_o)_{ZNMF} = (K^*)_{ZNMF} L^{-1/3} [\int F(T)dT]^{1/3} \tag{B.9}$$

APPENDIX C: EXPERIMENTAL DATA FOR PLUG PK-K-10-S-02-6.4 x 0.75

(raw data)

The tables contain the temperature differences across the plug and the superficial heat flux density (heat flow rate per total plug cross section).

ΔT,K	q,mW/cm^2
0.011	147.14
0.0198	211.88
0.0435	261.58
0.062	288.39
0.078	316.51
0.096	349.96
0.119	376.67

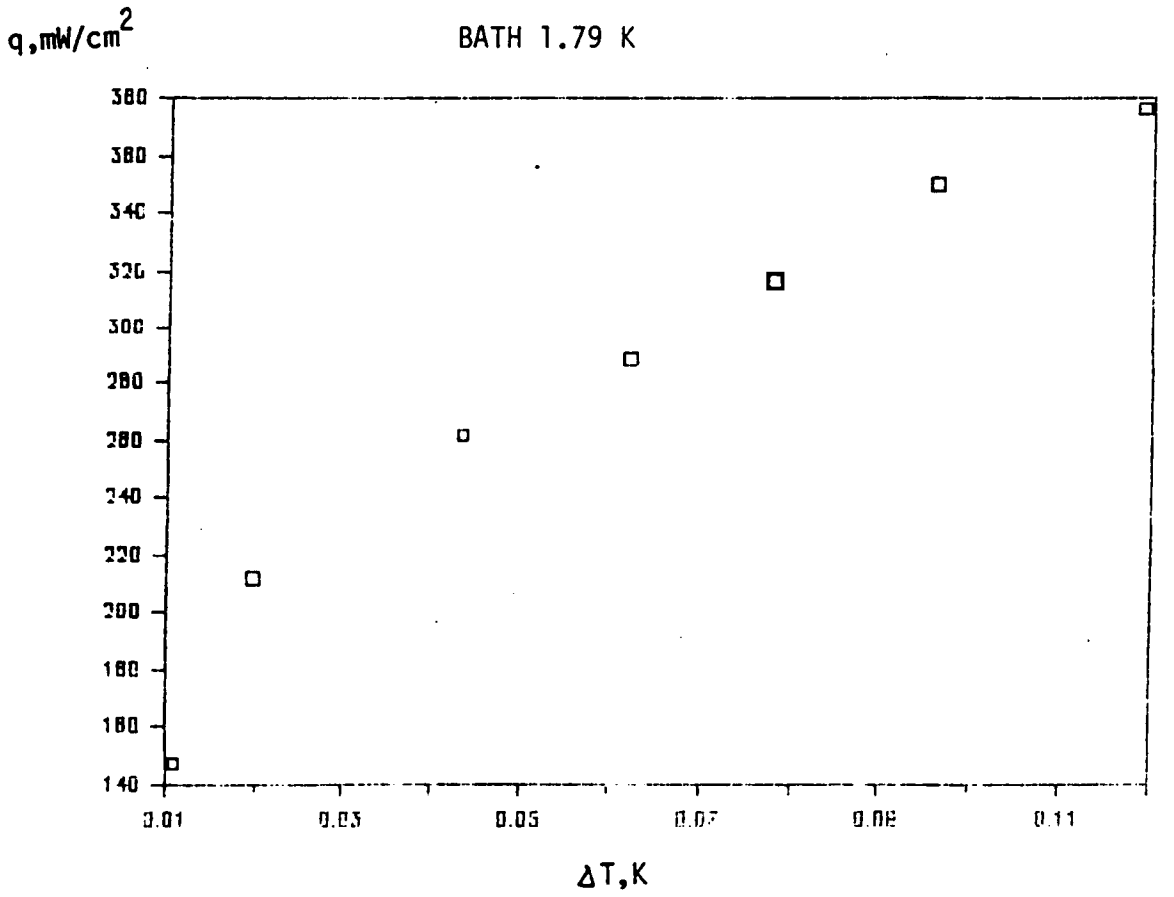

ΔT,K	q,mW/cm^2
0.00125	34.30000
0.00120	32.04000
0.00150	56.97000
0.00156	81.90000
0.00200	117.42000
0.00300	131.67000
0.00300	140.67000
0.00400	151.10000
0.00950	160.51000
0.01200	167.51000
0.01400	181.65000
0.01600	199.51000
0.01500	207.20000
0.02100	215.03000
0.02800	239.40000
0.03500	244.40000
0.05600	282.92000
0.05300	288.39000
0.08350	326.17000

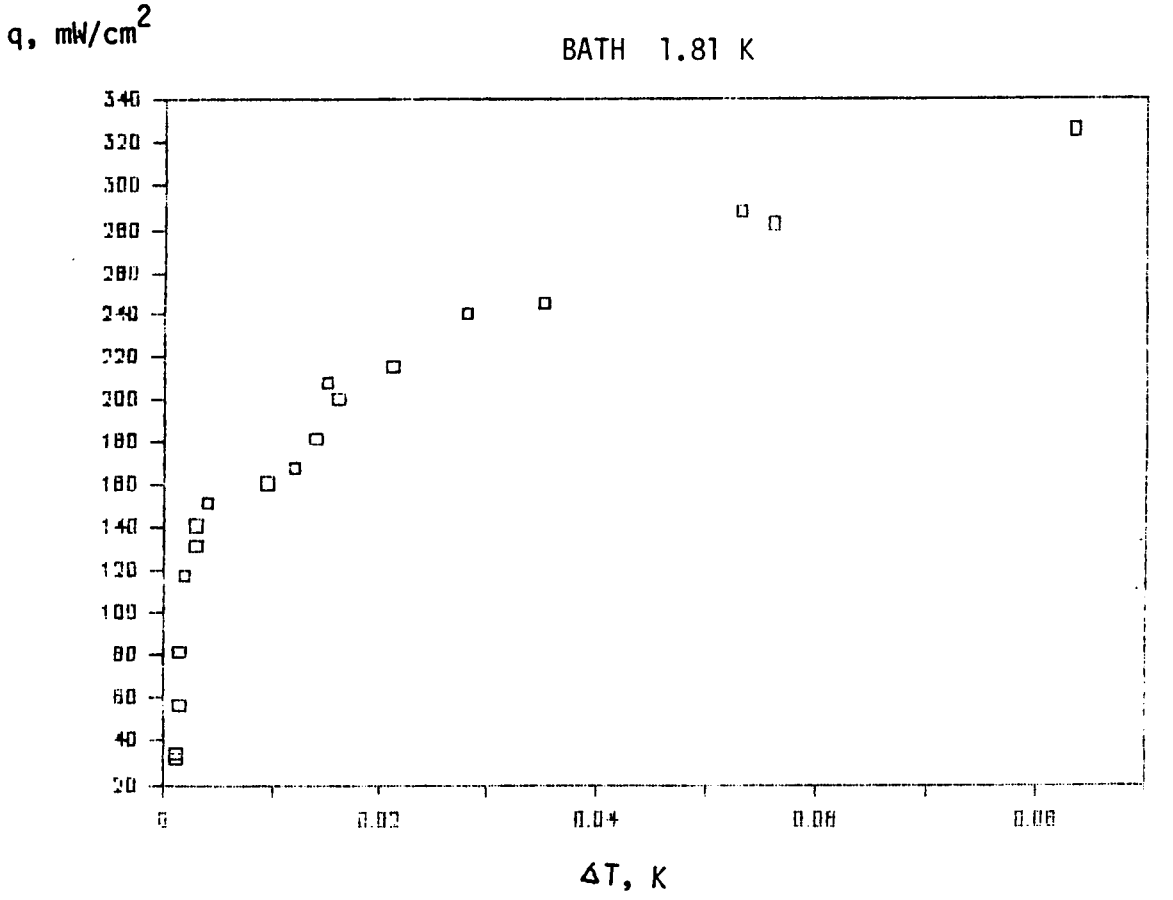

ΔT,K	q,mW/cm^2
0.0005	78.1700
0.0009	94.1700
0.0010	104.9000
0.0016	125.7400
0.0018	139.4000
0.0026	149.7700
0.0036	151.1000
0.0046	157.7800
0.0086	167.4100
0.0008	173.0400
0.0111	193.4600
0.0141	215.0000
0.0161	227.8600
0.0236	244.4300
0.0266	247.8100

T = 2.00 K

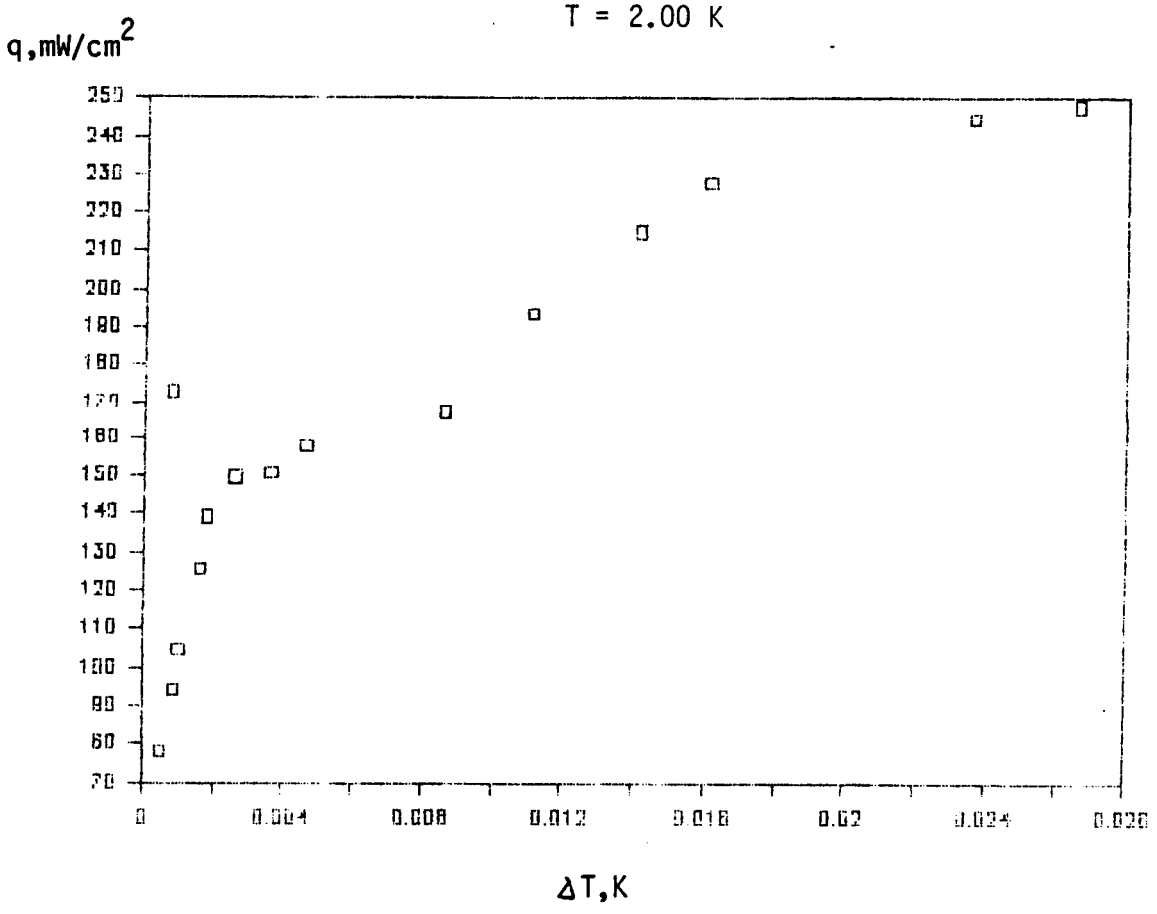

ΔT,K	q,mW/cm^2
0.0117	116.2600
0.0170	149.7700
0.0200	181.6500
0.0280	219.8000
0.0410	261.5800
0.0480	279.3100
0.0600	297.6200
0.1050	356.0400
0.1070	376.6700

q, mW/cm^2

BATH 1.88 K

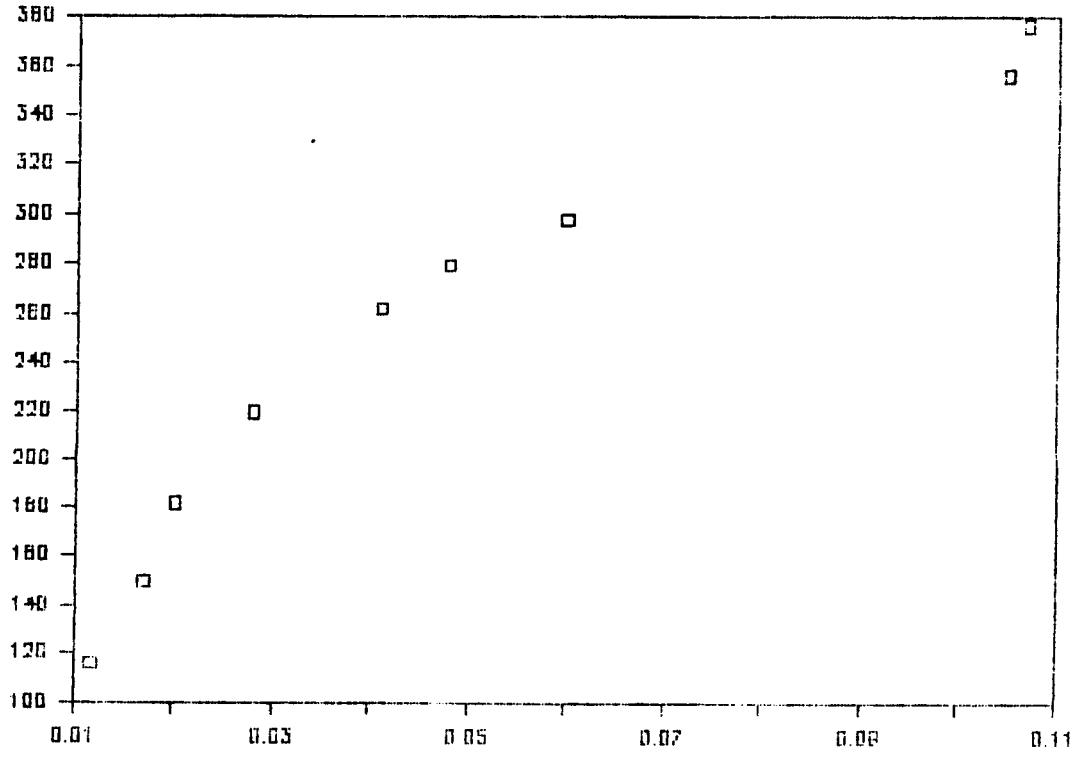

ΔT, K

ΔT,K	q,mW/cm^2
0.0030	13.4300
0.0040	39.7800
0.0050	45.9200
0.0050	65.3900
0.0055	68.9200
0.0065	88.0000
0.0075	98.4000
0.0090	112.7950
0.0110	122.1400
0.0125	125.7400
0.0165	144.5300
0.0255	164.6300
0.0310	178.6700
0.0450	199.5100
0.0620	231.1300
0.0940	279.3100
0.1160	295.7600
0.1300	314.6000
0.1660	347.9500

BATH 1.72 K

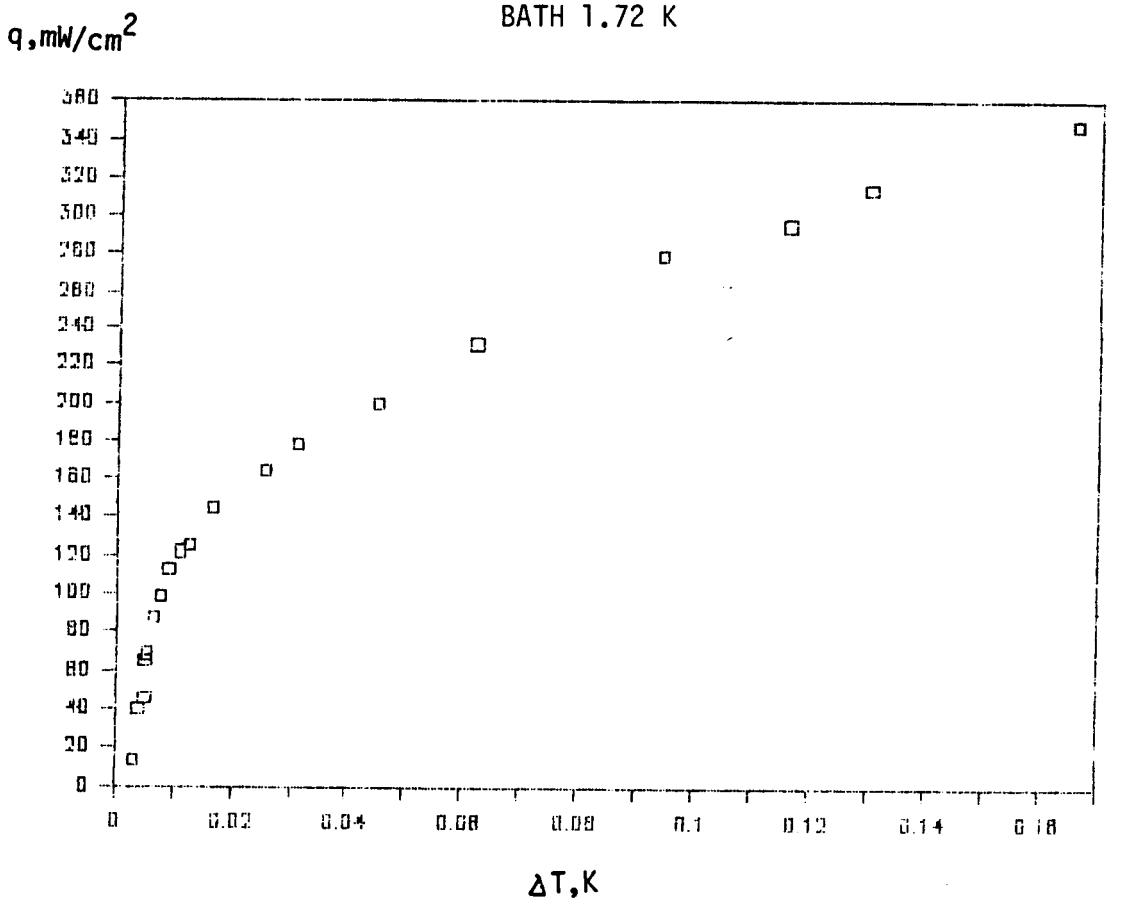

ΔT,K	q,mW/cm^2
0.0010	47.6100
0.0020	58.6100
0.0020	96.2700
0.0010	68.0300
0.0015	17.2300
0.0022	73.4100
0.0022	106.2700
0.0025	116.2500
0.0030	100.5500
0.0055	164.6300
0.0120	191.9700
0.0150	216.6100
0.0165	216.6100
0.0295	254.6500
0.0245	242.7500
0.0430	277.5100
0.0460	282.9200
0.0570	308.8900
0.0575	308.8900
0.0695	320.3600

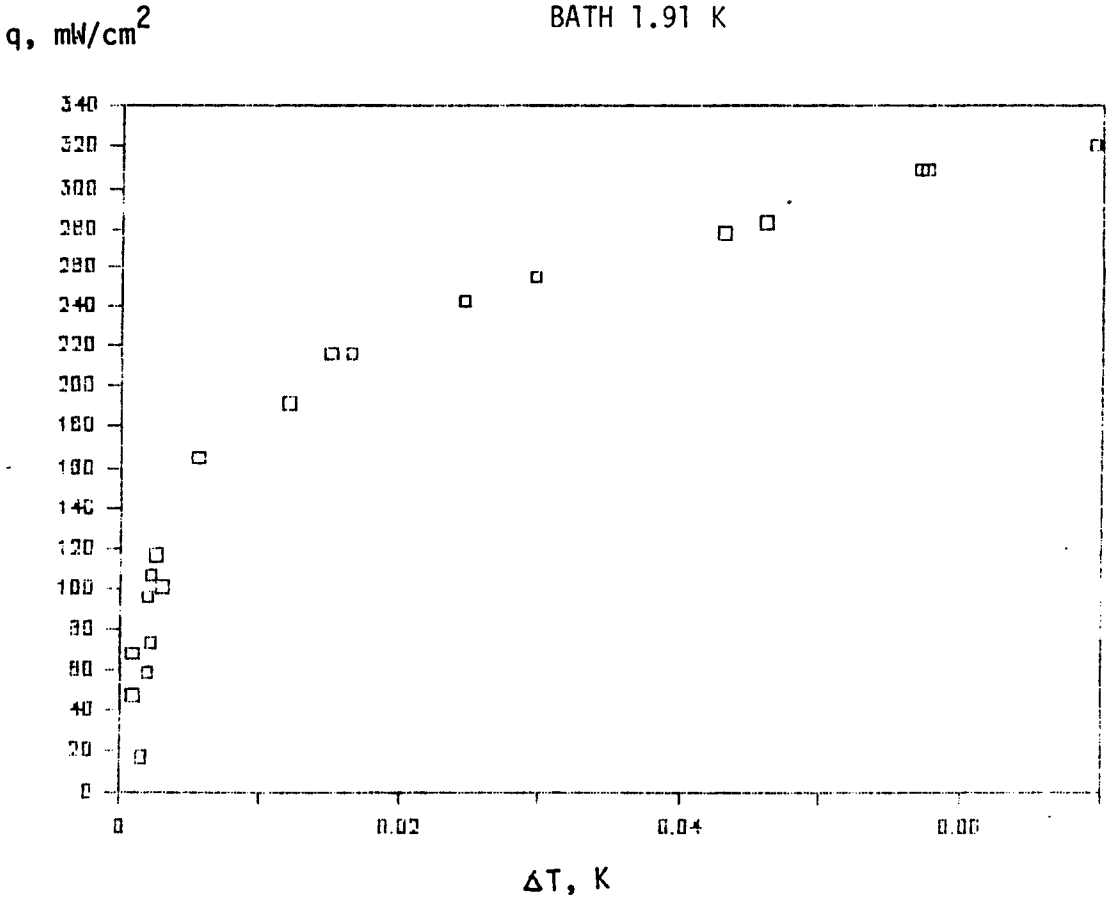

ΔT,K	q,mW/cm^2
0.0035	32.0400
0.0025	47.6400
0.0020	56.9700
0.0050	67.1500
0.0065	82.0300
0.0125	123.3400
0.0180	153.7500
0.0215	157.5900
0.0245	184.5700
0.0430	210.3100
0.0645	244.4300
0.0695	256.3700
0.1165	320.3600
0.1175	320.3600
0.1575	372.5000

BATH : 1.71 K

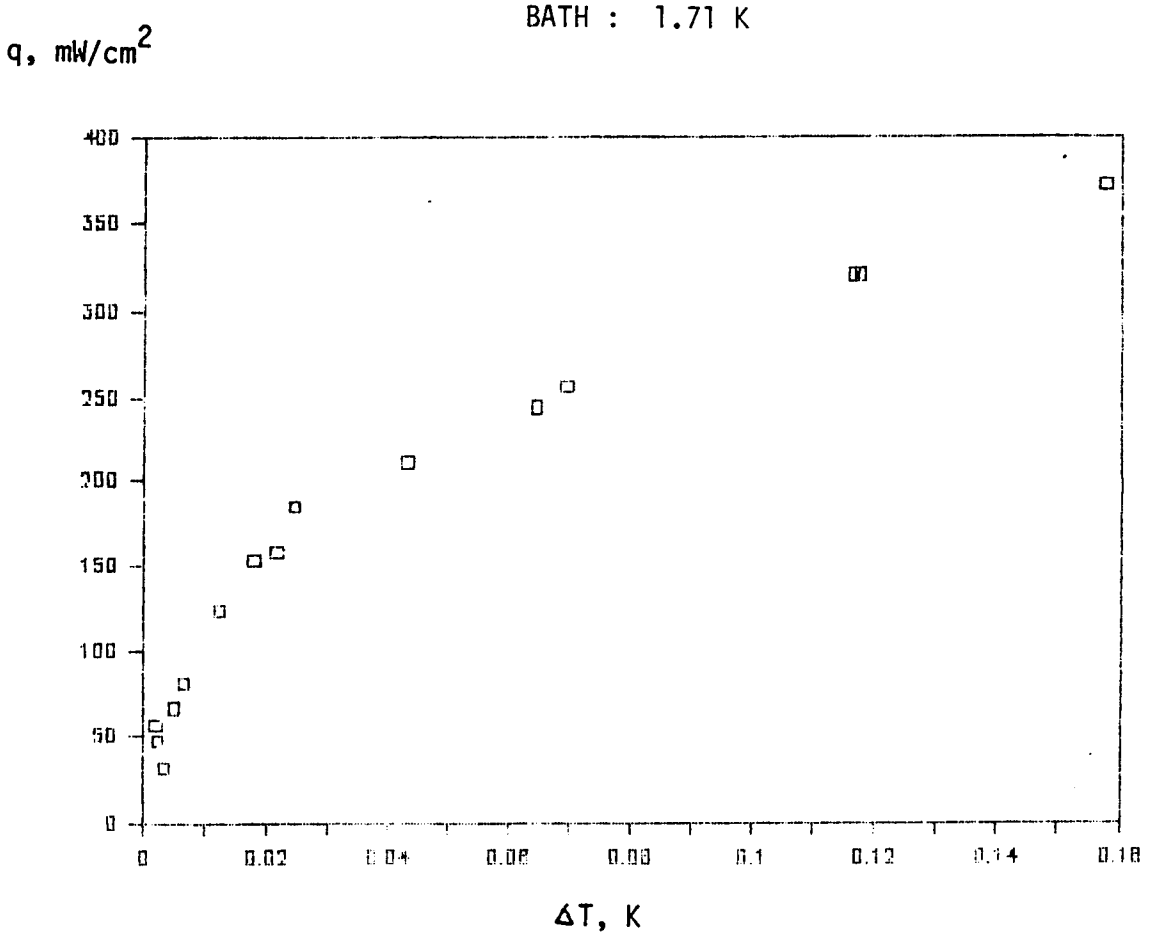

APPENDIX D: PERMEABILITY DETERMINATION

BASIC EQUATIONS

The permeability for ZNMF modes in the laminar region (i.e. low counterflow) is expressed within the generalized Darcy low as:

$$\overline{V}_{no} = \kappa_n \mid \nabla P_T \mid /\eta_n \qquad (D.1)$$

V_{no} = Initial normal fluid velocity

P_T = Thermomechanical pressure

η_n = Viscosity of normal fluid

κ_n = Permeability

London's equation predicts that the thermomechanical pressure gradient can be produced externally by a temperature gradient:

$$\nabla P = \rho S \nabla T \qquad (D.2)$$

ρ = Fluid density

S = Entropy

∇T = Externally applied temperature gradient

Finally, for ZNMF modes, the heat flux density (q_o) in the axial direction of flow through porous plugs is given by

$$\overline{q}_o = \rho \, ST\overline{v}_{no} \qquad (D.3)$$

so that through equations (D.1) and (D.2), the governing equation for permeability calculations in ZNMF is presented as:

$$\overline{q}_o = \rho ST \, \kappa_n \, \rho S \, (\Delta T/L)/\eta_n \qquad (D.4)$$

where often $\Delta T << T$, and there is a property function

$$f(T) = \rho^2 S^2 T/\eta_n \qquad (D.5)$$

APPENDIX E

THERMOMETER CALIBRATION AT VERY SMALL TEMPERATURE DIFFERENCES

The carbon resistor thermometers used are Allen - Bradley, 39 Ohm, resistors. The calibration procedure involves the measuring of the thermometer's resistance and the corresponding vapor pressure of the system. The properties of the thermometer are such that the resistance is approximately logarithmically proportional to the vapor pressure. This can be expressed as:

$$\ln (R) = a \ln (Pv) + b \qquad (E.1)$$

R = Thermometer resistance
Pv = Vapor pressure
a,b = Linear least square parameters

Therefore, by using a temperature-vapor pressure curve, such as the T-58 scale, the temperature versus resistance relationship is derived for small temperature difference. A printout of a sample computer program and its output shows the utilization of a T-58 cubic spline fit (fit presented by Donnelly, R.J., et al in *J. Low Temp. Phys., 1981)* for iterative resistance-temperature calculations

For very small T-differences, the calibration equation (.1) Permits a convenient determination of ΔT from the resistance difference ΔR. The slope of the vapor pressure curve is known from the T-58 scale:

$$\Gamma = P_v^{-1} \, dP_v/dT \qquad (E.2)$$

Inserting d ln R/d ln Pv = a = $(dR/R)/(dP_v/Pv)$ one obtains

$$\Delta T \cong \Delta R \, dT/dR = \Delta R \, (aR\Gamma)^{-1} \qquad (E.3)$$
$$\Delta T << T$$
$$R = R_0$$

$R = R_0$ at the bath temperature.

APP. D : (contin.) ,
SUBJECT : CUBIC SPLINE FITS TO
THERMOPHYSICAL FUNCTIONS

Example : ABOVE THE LAMBDA TRANSITION

Lit.: C.F. Barenghi, P.G.J.Lucas,
R.J. Donnelly, J.Low Temp.
Phys. 44, 491, 1981 .

Selected smooth spline fit results:

Spec.heat at vapor pressure of saturated
liquid , 4 internal knots, basis : T-58
scale; C sat in J/(mol K)

$T - T_\lambda$, K	T, K	Csat
10E-4	2.1721	45.777
10E-3	2.173	33.537
10E-2	2.182	21.222

The corresponding Prandtl numbers (Pr)
are 0.2691 , 0.5487, 0.7685 .

- - - - - - - - - - - - - - - -

T-58 SPLINE FIT : C.F. BARENGHI, R.J. DONNELLY,
R.N. HILLS, J. LOW TEMP. PHYS. 51,319,1983.

APPENDIX F. ABSTRACTS OF RECENT CONFERENCES

Am. Phys. Soc., Div. of Fluid Mechanics,
40th Annual Meeting, Eugene Oregon, 22-24.
Nov. 1987.

Non-Linear Counterflow in Porous Media*

HI 6

Nonlinear Counterflow in Porous Media. P. K. KHANDHAR and T. H. K. FREDERKING, University of California, Los Angeles, CA 90024 - Sintered stainless steel plugs have been subjected to counterflow using liquid He II at zero net mass flow (ZNMF). The normal fluid flow, emitted from a heater, is compensated for by an inflow of superfluid into the heating chamber. The results give a permeability on the order of 10^{-10} cm^2 in the linear region based on a Darcy law analog (nominal filtration rating near 1 μm of classical fluid flow through the sintered plugs). The non-linear region established at increased heater power is characterized by a ZNMF rate constant K^* (Gorter-Mellink mutual friction constant). In contrast to the wide duct value, the present K^* data are pore size dependent. K^* is found to be a monotonically increasing function of the permeability in qualitative agreement with porous plug data for vapor-liquid phase separation (VLPS). VLPS results for K^* have been found to be proportional to the square root of *permeability*[1].

[1]S. W. K. Yuan, Ph.D. Thesis, UCLA, 1985.

*) Supported in part by NASA AMES Research Center.

PERFORMANCE TEST OF A LABORATORY PUMP FOR LIQUID TRANSFER BASED ON THE FOUNTAIN EFFECT

W.E.W. Chen, T.H.K. Frederking and W.A. Hepler

University of California, Los Angeles
Los Angeles, Callifornia

ABSTRACT

A laboratory scale pump has been tested in detail in order to determine the flow characteristics of a heater-activated all-metal thermomechanical pump (fountain effect pump FEP). The emphasis is on the functional dependence of the fountain pressure difference versus mass throughput. A modified Vote et al. power law approximation is employed for a simplified description of the flow rate as a function of the driving force. Flow rates of up to 10 Litres/(hr cm^2) have been obtained despite a large nominal pore size of the porous plug of 2 μm (filtration rating) used for the FEP.

1987 Cryog. Eng. Conf. St. Charles, IL; June 1987, paper BC-6

APPENDIX G

REFRIGERATION AND HEAT PUMP SYSTEMS BASED ON He II VORTEX CONTROL*

T.H.K. Frederking, H.H.D. Tran and R.M.Carandang

University of California, Los Angeles 90024 CA

The utilization of thermomechanical forces permits pressure increases in pumps without moving parts. This topic has become an interesting option for liquid transfer at microgravity. In addition, the thermomechanical pump (fountain effect pump) may be used to energize refrigerators, substituting for the usual mechanical pump. In the present thermodynamic studies, cyclic variations of the fluid equilibrium state are investigated including performance parameters. In contrast to attainment of low temperatures, the emphasis is on heat pumping tasks at temperatures between 1.5 K and the lambda temperature.

Key words: He II; thermodynamic cycles ; fountain effect; refrigerator/heat pump systems.

1. Introduction

Increased use of liquid He II as a coolant near 1.8 K has included application of the fountain effect (thermomechanical effect). Examples are vapor-liquid phase separators and fountain effect pumps (FEP). Another type of application addressed in the present studies is the use of FEP - induced pressurization for refrigeration purposes and heat pumping. An original version of such a system, based on the control of the dynamics of quantized vortices, has been proposed and tested by Staas and Severijns [1] [1]. This Staas-Severijns cooler has aimed at the attainment of low temperatures down to 0.7 K . In contrast, the present work emphasizes heat pumping in the range of the temperature (T) encountered in space cryogenics and in superconducting magnets for high magnetic fields based on NbTi/Cu. The system applicability

[1] Numbers in brackets refer to the literature references listed at the end of this paper.

*) Presented at 4th Intern. Cryocooler Conf. Easton, Md. 1986.

Therefore, heat is to be removed in order to keep temperatures, at a specified location, time - independent. In the aftercooler (AC), the temperature is brought back to the bath temperature. In the "expander", application of the pressure difference generated in the FEP, forces superfluid through the plug. This results in cooling by the mechano-caloric effect. The refrigeration load (Q_R) is supplied in the cold box (CB). Finally, the capillary (CAP) connects the cold box to the bath.

Figure 2 indicates a scheme with a valve (V) replacing the capillary system. In principle, other means are available, e.g. a valve at the inlet. This option is not favored for a saturated liquid bath, as it may lead to pressure reduction and cavitation. This danger is avoided with pressurized liquid He II . It is noted that in Reference [1] a set of capillaries has been employed in order to test the flow conditions in the entropy carrying tubes downstream of the cold box.

4. Fountain Effect Pump Performance

The fountain effect unit is the driver for the vortex refrigerator. Therefore, its performance exerts an important influence on the coefficient of performance (COP) of the refrigeration process. Recent work on FEP use for liquid transfer in space [3] has prompted a critical inspection of various performance measures . Two types of effectiveness or efficiency figures have become known. One relates to the liquid yield, ultimately available at the receiver, during transfer from one vessel to another one. The other measure is the energetic effectiveness ε_e . Because of generally small values obtained for ε_e , there has been a sufficient incentive to improve the energetics of the FEP , e. g. by heat pump - assisted FEP units [4]. Ideal changes of state at $d\mu=0$ are referred to in the subsequent discussion of the FEP.

The energetic effectiveness is defined as the ratio of the flow power at the pump outlet , $\dot{W}_F$, to the heat input rate , $\dot{Q}$, energizing the pump. Neglecting the

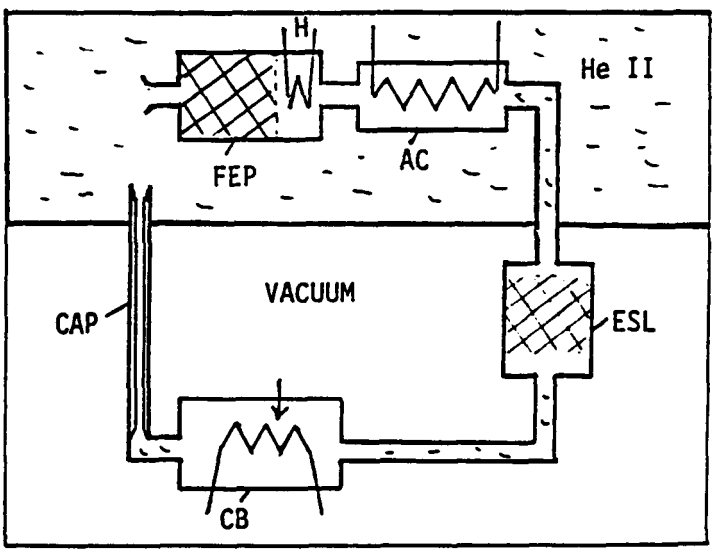

Figure 1. Vortex refrigerator, schematically; AC aftercooler, CAP capillary, CB cold box , ESL "expansion superleak", FEP fountain effect pump, H heater ; Refrigeration load Q_R is absorbed in the cold box.

$$\text{grad}\ (\mu + v_s^2/2) = 0 \qquad (2)$$

where the kinetic term is small outside the narrow passages formed by the porous medium. The momentum equation of the model , $\vec{J} = \rho\,\vec{v} = \rho_s\,\vec{v}_s + \rho_n\,\vec{v}_n$, for normal fluid locked in the plug, reduces to the simple condition

$$\rho\,\vec{v} = \rho_s\,\vec{v}_s \qquad (3)$$

Thus, the superfluid critical speed v_{sc} is related to the critical velocity of the observed mass flow by $v_c = v_{sc}\,\rho_s/\rho$.

In the terrestrial gravity field, the fountain effect is quantified readily by inclusion of the gravitational contribution to the generalized chemical potential function ($\mu + g\Delta z + v_s^2/2$) ; (z vertical position coordinate). In a thermo - static device, Equations (1) and (2) have in common the limit of the thermomechanical gradient, at zero flow, of

$$\text{grad}\ P = \text{grad}\ P_T = \rho\ S\ \text{grad}\ T \qquad (4)$$

(London pressure gradient). When a jet geometry allows a speed v , downstream of the superleak, the limit of ideal flow without losses leads to a fountain height of $\Delta z = v^2/(2\,g)$.

There are two types of fluid processing components in general: First, the porous plugs needed for the thermomechanics and second, ducts and conventional devices, such as heat exchangers. In the latter category, significant vortex shedding may take place causing dissipation of flow power. At sufficiently high flow rates, both fluids may move with nearly the same speed. In this case, interaction of the normal fluid with the vortices causes "near - classical " flow. For instance, in a duct with a diameter beyond the order of 10^{-2} cm, roughness - dependent friction may be observed readily, as in Newtonian turbulent fluid flow . Therefore, classical equations have been used in the analysis of this aspect of the Staas-Severijns refrigerator [1] . Alternate use of vortex pinning components and of vortex shedding components implies controlled processing of vortex systems giving rise to the designation of "He II vortex refrigerator" , (or of " superfluid vortex fridge"). The various dissipation aspects in wide and narrow passages have been reviewed by Hammel [2] giving details of basic thermophysics of the He II modes of motion.

3. Simplified Vortex Refrigerator Operation: Concepts

In the discussion of this section, simplified refrigeration concepts are invoked. Up to this time, little has become known about performance figures. In line with applied thermodynamics conventions, the coefficient of performance is defined as the ratio of the refrigeration load to the net work. The thermal efficiency of thermal to mechanical energy conversion is defined as the ratio of the net work to the heat input. Macro-thermodynamics is used. For instance, at a superficial glance one may refer to the FEP device as "compressor". The reverse case of mechano-caloric cooling in a plug may be referred to as "expansion device", (or "ideal superleak expander"). Caution is needed though to avoid a literal interpretation in terms of classical ideas which may lead to non-physical consequences .

A schematic diagram of the original system of the Staas-Severijns vortex refrigerator is shown in Figure 1. There are "compressor" and "expander " peculiarities elucidated by the two-fluid model for du = 0 . "Compression" is actuated by the heater (H) which supplies thermal energy. As superfluid passes through the device at $d\mu = 0$, normal fluid left behind tends to accumulate entropy upstream.

appears to be not restricted to these examples and general features are presented: First, the vortex dynamics is discussed. Subsequently, simplified refrigerator operation is considered. The next subject is the FEP pressurization device. Heat pumping performance is considered for one of the simplest cycle options, and an outlook is given.

2. Vortex Dynamics and Two - Fluid Aspects

The quantum liquid He II has a high heat transport rate in conventional refrigerator ducts, unless the flow cross section is severely restricted. Therefore T - gradients are small in usual flow passages. In order to generate sizable temperature differences, needed for the application of thermomechanical forces, fine porous media, called superleaks or superfilters, are used. The limiting case is the "ideal superleak" with zero heat flow. The porous medium permits resistanceless flow (="superflow") up to its critical velocity (v_{sc}). As the pore size is reduced, at a specified temperature, the v_{sc} - value attainable is increased. At v_{sc}, liquid circulation and flow resistance is initiated. Because of quantization of the liquid circulation, a finite energy is needed for vortex motion onset with velocity components perpendicular to the main flow direction, i. e. vortex shedding . The energy needed is large for very fine pores. For FEP purposes, critical velocities of the order of 10 cm/s have been considered convenient in laboratory work. Because of the energetic restrictions, the fine plugs may be regarded as "vortex pinning devices" below v_{sc} . In the ideal thermodynamic treatment of changes of state, the ideal superleak constitutes a perfect vortex pinning component.

Once a vortex is activated above v_{sc} , a Magnus force provides vortex shedding e.g. from walls toward the fluid interior. This phenomenon leads to a finite difference in chemical potential (μ) *. In the ideal superleak $d\mu = 0$ is observed up to the critical velocity. Small vortex shedding rates of real plugs are expected to cause only small departures from the ideal thermodynamic change of state. Therefore, ideal processes involving changes of state at constant chemical potential are useful for performance assessment. It appears that minor vortex shedding rates cause only small departures from the ideal performance values of FEP units.

We have a flow system described in usual hydrodynamic terms supplemented by the superflow thermodynamics. The two - fluid model is useful . The existence of two interpenetrating fluid media is postulated: There exists a viscous normal fluid component and an inviscid superfluid component (at"concentrations " (ρ_n/ρ) and (ρ_s/ρ) adding up to unity). The flow field is subdivided accordingly: There is a normal fluid flow pattern and a superfluid flow field. Because of the fine pores, the normal fluid motion is considered negligible, in particular in the limit of perfect immobilization of superleaks. Thus, in the present context , attention is on the superfluid described by

$$D\vec{v}_s/Dt = -\nabla\mu = \nabla P/\rho - S\nabla T - (1/2)(\rho_n/\rho)\,|\vec{w}|^2 \qquad (1)$$

with $\vec{w} = \vec{v}_n - \vec{v}_s$ = relative velocity ; S entropy per unit mass; ρ liquid density). For steady, one-dimensional flow with negligible $|\vec{w}|^2$ term, we have a simple truncated form of the preceding equation

*) In part of the low temperature literature, the Gibbs free energy is customarily denoted as μ . In the present discussion , this notation is adopted with μ =chemical potential per unit mass.

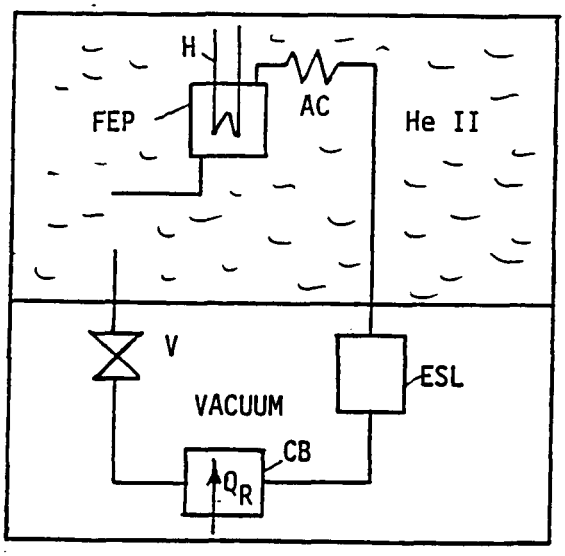

Figure 2. Vortex refrigerator, schematically; V valve, (other components as in Figure 1).

mass loss and using Equation (4), one obtains

$$\varepsilon_e = \dot{W}_F / \dot{Q} = \bar{S}\Delta T / S\,T \qquad (5)$$

$\bar{S}$ is the mean entropy for the range from the bath temperature T to the temperature $(T + \Delta T)$ at the pump exit. For very small temperature differences, $\bar{S}$ becomes equal to the bath value $S(T)$, and the effectiveness simplifies to

$$\varepsilon_e = \Delta T/T \quad ; \quad \Delta T \ll T \qquad (6)$$

A comparison with the thermal efficiency of a Carnot cycle shows that the FEP effectiveness, in this limit, is equal to that efficiency for a low temperature environment. More specifically, the comparison Carnot power cycle receives heat at the temperature $(T + \Delta T)$ and rejects heat at T.

Figure 3 presents a comparison of the FEP effectiveness with the thermal efficiency (η_T) of the related Carnot power cycle. According to Carnot's theorem, the η_T - values constitute the best performance results available ideally. It is seen that ε_e is always below η_T . The effectiveness is about 50 % lower than the Carnot limit. There is a common asymptote at low ΔT. The parameter adopted in Figure 3 is the bath temperature upstream of the FEP unit. At sufficiently high ΔT, the FEP performance tends toward an asymptote, near 15 % of the ideal heat pump-assisted FEP unit [4] .

Figure 4 shows the heater power requirements. Figure 4a is a plot of the heat input rate per mass flow rate $(\dot{Q}/\dot{m})$, starting at a temperature of 1.6 K versus the temperature difference across the ideal pump. The upper curve is the ideal requirement of the simple FEP . The real pump will need a somewhat larger power because of departures from the ideal change of state characterized by $d\mu = 0$. The lower curve depicts the power requirements, $\dot{W}/\dot{m}$, per unit mass, of the heat pump-assisted

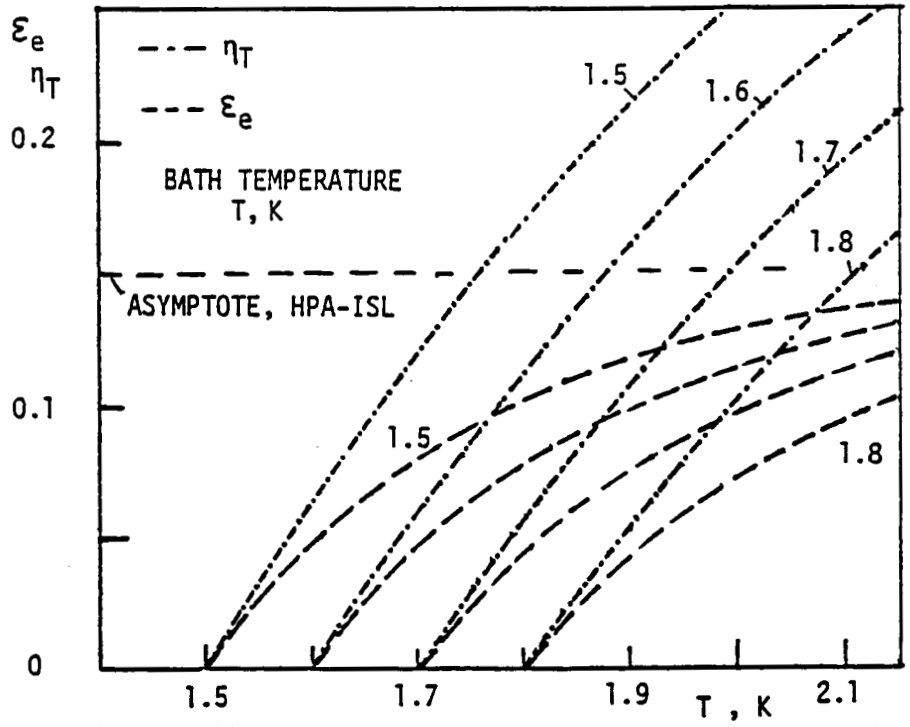

Fig.3. Energetic effectiveness ε_e and thermal efficiency η_T of ideal systems for various bath temperatures; (HPA-ISL heat pump-assisted ideal superleak).

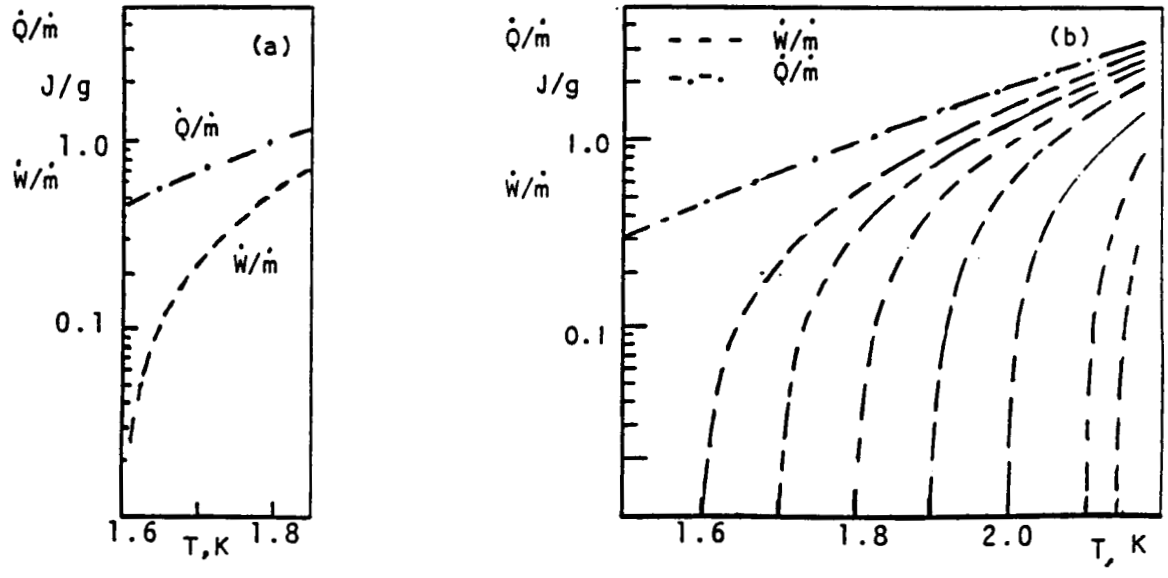

Fig.4. Heater input ($\dot{Q}/\dot{m}$) and power input ($\dot{W}/\dot{m}$) functions for ideal FEP systems; a. power required versus ΔT , bath temperature 1.6 K; b. parametric plot of the power required vs. T for various bath temperatures.

FEP unit. This power is low at low ΔT and rises monotonically with an increase in the temperature difference.

Figure 4b summarizes the power input requirements in one graph making use of a parametric representation with the bath temperature (upstream temperature) as parameter. It is seen that there is a unique ideal heater power function $(\dot{Q}/\dot{m})$ given by the ideal superleak constraint : $(\dot{Q}/\dot{m})$ is the value of S T at the pump exit. For instance, for a mass flow rate of $\dot{m}$ = 40 g/s , or a volumetric flow rate of about 1000 liters/hour, a heater power of the order of 40 Watts is required near 1.8 K. At large temperature differences, the heat pump assistance is no longer attractive as the power requirement approaches that of the simple FEP unit.

5. Refrigeration - Heat Pump Cycle Example

One important assumption in the preceding and in the present treatment is at - tainment of local thermodynamic equilibrium . Other system conditions of the present section are as follows: steady operation, steady flow of liquid and of the two fluids, simplified changes of state using ideal conditions, such as isobaric changes in heat exchangers, and ideal superleak processes at constant chemical potential. A simplifying tool is the introduction of the ideal heat pump-assisted FEP ($d\mu$= 0) and a related state change in the "expander " subsystem. Furthermore, for quick estimates the contribution from the integral $\int S\, dT$ may be neglected in the T-range near 1.8 K, as discussed elsewhere [4] . The changes of state are listed in Table 1.

TABLE 1 . STATE CHANGES OF THE SIMPLE CYCLE μ-P-μ-P

Sequence i - j	Constraint	Subsystem/Component
1 - 2	$d\mu = 0$	Ideal FEP,heat pump-assisted
2 - 3	$dP = 0$	Isobaric aftercooler ($T_3 = T_1$)
3 - 4	$d\mu = 0$	Ideal superleak"expander"
4 - 1	$dP = 0$	Absorption of the refrigeration load Q_R

The cycle is sketched in the T-S plane and in the P-T plane in the insets of Figure 5. After processing of fluid in the FEP, the aftercooler brings the temperature back to the bath temperature T_1. Subsequent "expansion" brings about a low temperature, and finally the change of state from T_4 to T_1 is assumed to be available for the absorption of the refrigeration load.

The temperature T_4 has been plotted for various pressure increases in Figure 5. For instance, the pressure rise in the FEP unit, starting from 1.8 K, produces a T_4 -value near 1.63 K; (pressure difference achieved across the FEP of about 100 milli-bar). Figure 5 includes the equivalent Carnot cycle temperature, for an "environment" of 1.8 K, which has the same refrigeration load as the μ-P-μ-P cycle under consideration. Both temperatures are displayed versus Q_R .

Coefficients of performance of the Carnot cycle $(COP)_{CARNOT}$ are shown in Fig.6 versus T . As the initial "environmental temperature" , e.g. 1.8 K , is lowered by a small reduction $\Delta T \ll T$, the COP is the reciprocal η_T - value of the power process.

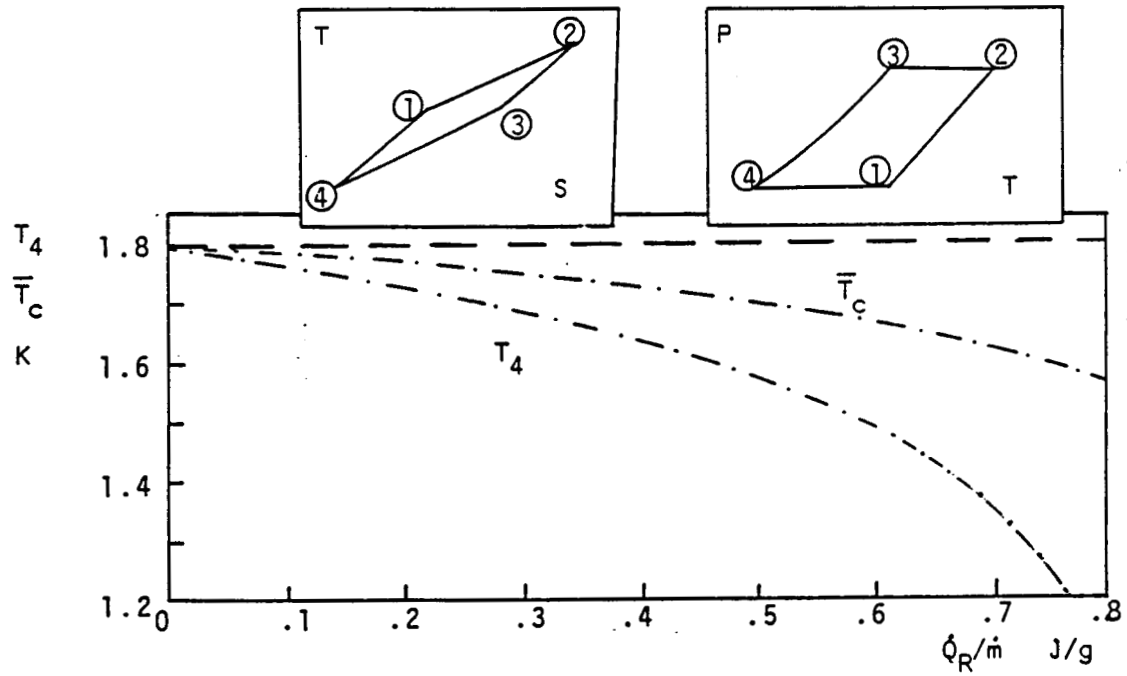

Fig.5. Lowest temperature T_4 of the ideal μ-P-μ-P cycle and equivalent Carnot cycle temperature $\bar{T}_c$ vs. refrigeration load $\dot{Q}_R/\dot{m}$; "environmental" T = 1.8 K = initial bath temperature T_1; inset : Cycle in the T-S diagram, schematically and cycle in the P-T diagram , schematically.

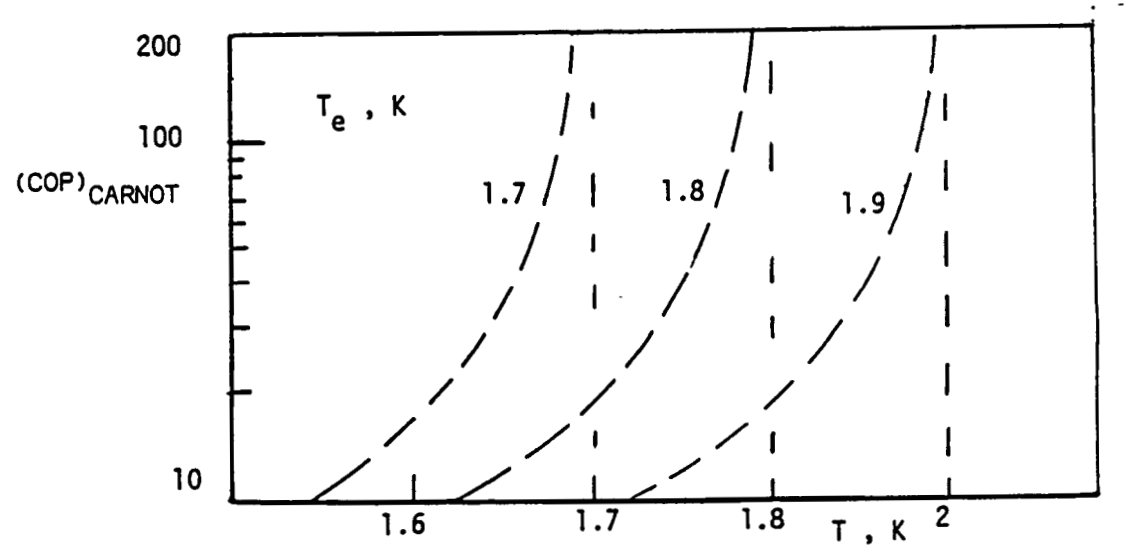

Fig. 6. Coefficients of performance of the Carnot cycle, $(COP)_{CARNOT}$ versus T for different"environmental temperatures" Te .

6. Perspectives

Simplified changes of state, with heat pump assistance of the FEP process, and a similar "expander assisted" pressure reduction, have been considered. The implementation of near - ideal conditions by external means may require considerable component developments. Therefore other approaches toward improvement of the very simple cycle ought to be considered. One possibility is a counterflow heat exchanger. Another one is via"Carnotization" by means of multi-stage operation.

Figure 7 depicts a schematic diagram of a vortex refrigerator with a counterflow heat exchanger increasing the T -range covered by the heat pump process. The counterflow avoids excessive entropy production brought about otherwise by a large temperature difference between the "high pressure" stream and the"low pressure" stream.

The other option of Carnotization is brought about by multi-stage "compression" and multi-stage"expansion" . Figure 8 presents an example of a three-stage FEP - system with aftercoolers (AC). The inset of this figure is a sketch of the multi-stage cycle . As the number of stages is increased, the Carnot case is approached more and more. While the low density change makes multi-stage "expansion"*less attractive, the possibility of multi-stage "compression" has received attention, e.g. Ref.[5] for the special case of He^3 - He^4 dilution refrigeration, and Reference [6] for the T-range near 1.8 K in the space cryogenics work of recent years.

In the final assessment, a major point is the FEP performance. The ideal energetic effectiveness figures of at most 15 % are not very attractive. A major advantage of the FEP - supported system is the generally high reliability due to the absence of moving components (aside from valve positioning). The most attractive issue appears to be the possibility of"waste heat"utilization (e.g. vessel heat leaks, instrument dissipation rates). For high field magnets, an example of liquid circulation has been presented in Ref.[7].For space cryogenics systems, the use of a cooler-activated FEP unit is a viable option. Also heat might be"piped" from solar energy concentrators to the FEP without the use of photo-voltaics. Further recent results are in Ref. [8] .

In summary, attractive features of the He II thermomechanics are available for specific refrigeration and heat pumping tasks.

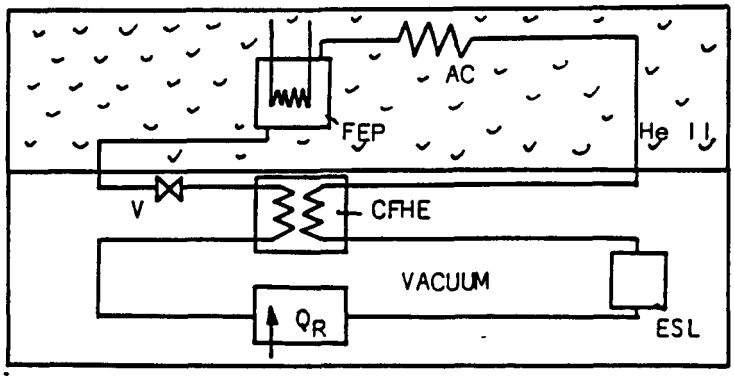

Figure 7 . Vortex refrigerator with a counterflow heat exchanger (CFHE), schematicaly; AC aftercooler , CB cold box ; ESL "expansion superleak" , FEP fountain effect pump with heater; V valve .

*) from a "classical" point of view.

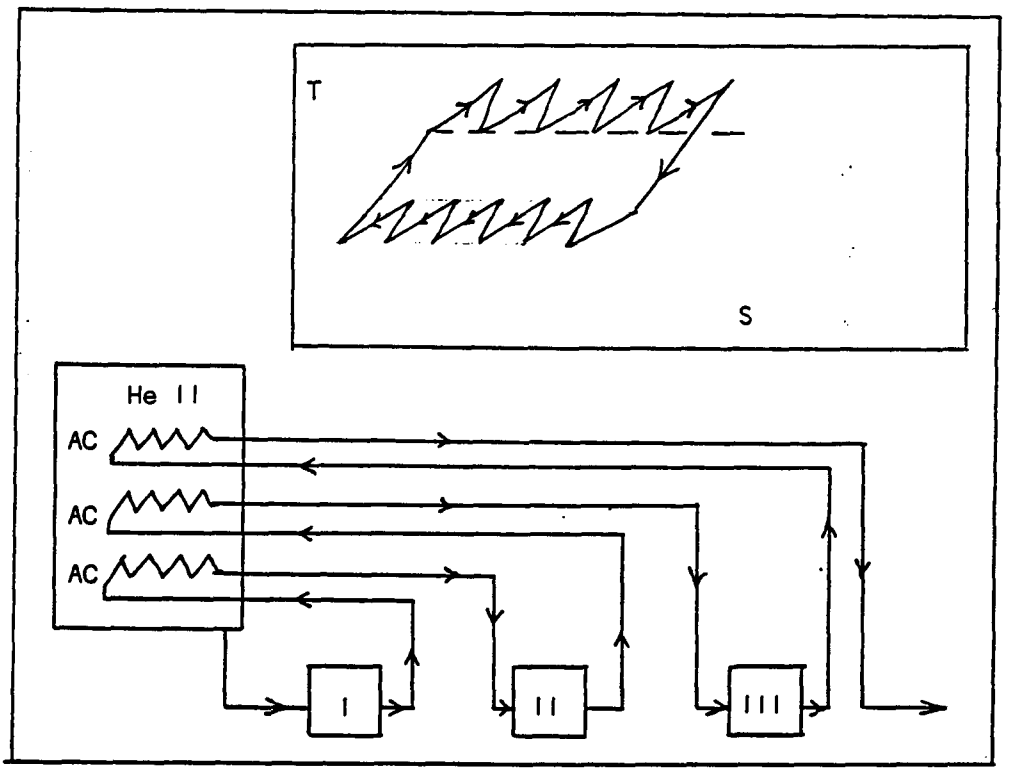

Figure 8. Example of multi-stage "compression" with three stages of FEP units designated as I, II, III ; AC after coolers in He II supply tank (schematically ; inset : Temperature - Entropy diagram for multi-stage "compression and "expansion" , schematically.

Acknowledgments. This work has received initial "seed" support from the Academic Senate Grant # 3526 , UCLA. Also NASA Summer 1986 support in the area of thermal components is acknowledged in this context (# NAG 2 - 412). The following students participated in the efforts : Kenny Hom, Alana Lee and David Ono. Their input is recognized with thanks. Further the help of Y.S. Yi is gratefully acknowledged.

7. References

[1] Staas F.A. and Severijns, A.P., Vorticity in He II and its Application in a Cooling Device, Cryogenics 9, 422 - 426 (1969).

[2] Hammel, E.F., Dissipation and Critical Velocities in Liquid Helium, LT-10, 10th Int. Conf. Low Temp. Phys. 1966, plenary paper.

[3] Kittel, P. , Helium Transfer in Space Workshop, Cryogenics 26, 59-60 (1986).

[4] Frederking, T.H.K. et al., Fountain Effect-Based Cycles and Related Changes of State, paper 07-4, ICEC-11, 11th Int. Cryog. Eng. Conf. Berlin 1986.

[5] Severijns, A.P., A Novel He^3-He^4 Dilution Refrigerator with Superfluid He^4 Circulation, Cryogenics 20, 115 - 121 (1980).

[6] Kittel, P. Liquid Helium Pumps for in Orbit Transfer, Space Cryog. Workshop,

Noordwijk, Holland, April 1986.

[7] Hofmann, A., Thermomechanically Driven He II Flow, An Option for Fusion Magnets with Internally Cooled Conductors, ICEC-11, 11th Int. Cryog. Eng. Conf. Berlin 1986.

[8] Hofmann, A. Khalil A., Kraemer, H.P. , Weisend, J.G., Srinivasan, R. and Vogeley, B., Investigations of Fountain Effect Pumps for Circulating Pressurized Helium II, ICEC-11, 11th Int. Cryog. Eng. Conf. Berlin 1986.

ADDITIONAL COMMENTS

Numerous details of dissipative processes including narrow duct phenomena have been presented in the survey paper of E. F. Hammel at the Int. Conf. Low Temp. Phys. LT-10 , 1966 . This work has been based on the extensice studies of Keller and Hammel (also documented in the monograph of W.E. Keller on Helium-3 and Helium-4, Plenum Press 1969.

Concerning thermodynamic efficiency figures and similar measures, H.B. Callen*presents several examples : (simplified expressions on the right hand side are Carnot values)

Thermodynamic engine efficiency

$$\varepsilon_e = d W / |-d Q_H| = 1 - T_C/T_H$$

Coefficient of refrigerator performance

$$\varepsilon_r = |- dQ_C| / |- d W| = T_C / (T_H - T_C)$$

Coefficient of heat pump performance

$$\varepsilon_p = dQ / |- dW| = T_H / (T_H - T_C)$$

---

*) THERMODYNAMICS AND AN INTRODUCTION TO THERMOSTATISTICS, 1985, John Wiley, New York.